Event-based update of synapses in voltage-based learning rules

Jonas Stapmanns [1,2,*], **Jan Hahne** [3], **Moritz Helias** [1,2], **Matthias Bolten** [3], **Markus Diesmann** [1,4,5] **and David Dahmen** [1]

[1] *Institute of Neuroscience and Medicine (INM-6) and Institute for Advanced Simulation (IAS-6) and JARA Institute Brain Structure Function Relationship (INM-10), Jülich Research Centre, Jülich, Germany*
[2] *Institute for Theoretical Solid State Physics, RWTH Aachen University, Aachen, Germany*
[3] *School of Mathematics and Natural Sciences, Bergische Universität Wuppertal, Wuppertal, Germany*
[4] *Department of Physics, Faculty 1, RWTH Aachen University, Aachen, Germany*
[5] *Department of Psychiatry, Psychotherapy and Psychosomatics, Medical Faculty, RWTH Aachen University, Aachen, Germany*

Correspondence*:
Jonas Stapmanns
jonas.stapmanns@rwth-aachen.de

ABSTRACT

Due to the point-like nature of neuronal spiking, efficient neural network simulators often employ event-based simulation schemes for synapses. Yet many types of synaptic plasticity rely on the membrane potential of the postsynaptic cell as a third factor in addition to pre- and postsynaptic spike times. Synapses therefore require continuous information to update their strength which a priori necessitates a continuous update in a time-driven manner. The latter hinders scaling of simulations to realistic cortical network sizes and relevant time scales for learning.

Here, we derive two efficient algorithms for archiving postsynaptic membrane potentials, both compatible with modern simulation engines based on event-based synapse updates. We theoretically contrast the two algorithms with a time-driven synapse update scheme to analyze advantages in terms of memory and computations. We further present a reference implementation in the spiking neural network simulator NEST for two prototypical voltage-based plasticity rules: the Clopath rule and the Urbanczik-Senn rule. For both rules, the two event-based algorithms significantly outperform the time-driven scheme. Depending on the amount of data to be stored for plasticity, which heavily differs between the rules, a strong performance increase can be achieved by compressing or sampling of information on membrane potentials. Our results on computational efficiency related to archiving of information provide guiding principles for the future design of learning rules in order to make them practically usable in large-scale networks.

Keywords: voltage-based plasticity rules, event-based simulation, spiking neural network simulator, NEST, Clopath rule, Urbanczik-Senn rule

1 INTRODUCTION

One mechanism for learning in the brain is implemented by changing the strengths of connections between neurons, known as synaptic plasticity. Already early on, such plasticity was found to depend on the activity

of the connected neurons. Donald Hebb postulated the principle 'Cells that fire together, wire together' (**Hebb**, 1949). Later on, it was shown that plasticity is shaped by temporal coordination of activities even down to the level of individual spikes (**Markram et al.**, 1997; **Bi and Poo**, 1998). Synaptic plasticity rules for spiking neural networks, such as spike timing-dependent plasticity (STDP, **Gerstner et al.** (1996)), consequently employ spike times of pre- and postsynaptic cells to predict the change in connections.

In recent years, a new class of biologically inspired plasticity rules has been developed that take into account the membrane potential of the postsynaptic neuron as an additional factor (for a review, see **Mayr and Partzsch**, 2010; **Gerstner et al.**, 2014). The rule by **Clopath et al.** (2010) can be seen as a prototypical example for a voltage-based plasticity rule since long-term potentiation of synapses depends on the presynaptic spike arrival and a filtered version of the postsynaptic membrane potential. This additional voltage dependence enables the Clopath rule to describe phenomena that are not covered by ordinary STDP but can be observed in experimental data, such as the complex frequency dependence of the synaptic weight changes in spike pairing experiments (**Sjöström et al.**, 2001). Furthermore it provides a mechanism for creation of strong bidirectional connections in networks, which have been found to be overrepresented in some cortical areas (**Song et al.**, 2005).

Further inspiration for recently proposed plasticity rules originates in the field of artificial neural networks. The latter showed great success in the past decade, for example in image or speech recognition tasks (**Hinton et al.**, 2006; **Krizhevsky et al.**, 2012; **Hannun et al.**, 2014; **LeCun et al.**, 2015). The involved learning paradigms, for example the backpropagation algorithm (**Werbos**, 1974; **Parker**, 1985; **Lecun**, 1985; **Rumelhart et al.**, 1986), are, however, often not compatible with biological constraints such as locality of information for weight updates. To bridge the gap to biology, different biologically inspired approximations and alternatives to the backpropagation algorithm have been proposed (**Sacramento et al.**, 2018; **Bellec et al.**, 2019). A common feature of these rules is that weight updates not only depend on the output activity of pre- and postsynaptic cells, but also on a third factor, which is a time-continuous signal. A prominent example of such biologically and functionally inspired rules is the voltage-based plasticity rule proposed by **Urbanczik and Senn** (2014), where the difference between somatic and dendritic membrane potential serves as an error signal that drives learning. This rule, incorporated in complex microcircuits of multi-compartment neurons, implements local error-backpropagation (**Sacramento et al.**, 2018).

Research on functionally inspired learning rules in biological neural networks is often led by the requirement to implement a particular function rather than implementation efficiency. Present studies are therefore primarily designed to prove that networks with a proposed learning rule minimize a given objective function. Indeed many learning rules are rather simple to implement and to test in ad-hoc implementations where at any point the algorithm has access to all state variables. While the latter implementations are sufficient for a proof of principle, they are hard to reuse, reproduce and generalize. In particular, simulations are restricted to small network sizes, as the simulation code cannot be straight-forwardly distributed across compute nodes and thus parallelized. This is, in particular, problematic given that successful learning requires extended simulation times compared to the update interval.

In parallel to the above efforts are long-term developments of simulation software for biological neural networks (**Brette et al.**, 2007). Such open-source software, combined with interfaces and simulator-independent languages (**Davison et al.**, 2008; **Djurfeldt et al.**, 2010, 2014), supports maintainability and reproducibility, as well as community driven development. The design of such simulators is primarily led by implementation efficiency. Code is optimized for neuron and synapse dynamics, with the aim to upscale simulations to biologically realistic network sizes. A modular structure of the code facilitates re-use and

extensions in functionality. Therefore, one aim of the community should be the transfer of ad-hoc proof-of-principle implementations to these well-tested platforms. Given the differences in design principles behind the exploratory development of specific models and general-purpose simulation technology, this transfer is not trivial. In the current study, we show how to make voltage-based learning rules compatible with spiking neural network simulators that employ an event-driven update scheme of synapses.

Modern network simulators use individual objects for different neurons and synapses, which allows the distribution of large networks across many compute processes (**Jordan et al.**, 2018; **Lytton et al.**, 2016). Spiking simulators in addition idealize spikes as point-like events. In the absence of gap junctions, there is no neuronal interaction in between such spike events such that neuronal and synaptic state variables can be propagated independently in time. This led to the development of event-based simulation schemes, where synapses are only updated in their state at the times of incoming spikes (**Morrison et al.**, 2005). Since spike events at single synapses are rare for physiological brain states, this significantly reduces the amount of function calls to synapse code and optimizes computational performance in network simulations. Such an event-based scheme is perfectly suitable for plasticity rules like STDP, which rely on a comparison between two point-like events. However, in voltage-based learning rules, synapses continuously require information from the postsynaptic neurons in order to update their weights. This a priori breaks the idea behind an event-based update scheme.

In this study we present an efficient archiving of the history of postsynaptic state variables that allows for an event-based update of synapses and thus makes voltage-based plasticity rules compatible with state-of-the-art simulation technology for spiking neural networks. In particular, we derive two event-based algorithms that store a time-continuous or discontinuous history, respectively. The latter relies on a compression of information at the time of spike events and is beneficial for learning rules that require the storage of long histories. We theoretically analyze advantages of the two event-driven algorithms with respect to each other and compared to a straight-forward time-driven algorithm.

The presented simulation concepts are exemplified and evaluated in a reference implementation in the open source simulation code NEST (**Gewaltig and Diesmann**, 2007; **Jordan et al.**, 2019). The reference implementation thereby exploits existing functionality of a scalable software platform which can be used on laptops as well as supercomputers. NEST is employed by a considerable user community and equipped with an interface to the programming language Python (**Eppler et al.**, 2009), the field of computational neuroscience has agreed on. It supports relevant neuron models and connection routines for the construction of complex networks. Despite this flexibility the simulation engine shields the researcher from the difficulties of handling a model description in a distributed setting (**Morrison et al.**, 2005; **Plesser et al.**, 2015).

We here focus on the voltage-based plasticity rules by **Clopath et al.** (2010) and **Urbanczik and Senn** (2014). The two rules represent opposing ends of a family of learning rules in the amount of data required to compute weight updates. The Clopath rule by design only triggers plasticity in the vicinity of postsynaptic spike events; storing a history, which is non-continuous in time, thus becomes beneficial. In contrast, the Urbanczik-Senn rule considers noisy prediction errors based on postsynaptic membrane voltages and spikes. Such prediction errors never vanish and therefore always need to be stored to update the weights, leading to time-continuous histories. For a given span of biological time, simulations of the Urbanczik-Senn rule are therefore by design less efficient than those of the Clopath rule. However, we show that a compression of membrane potential information reduces this performance gap. Changing the learning rule to include a sparse sampling of the membrane voltage further increases efficiency and makes performance comparable to simulations with ordinary STDP.

Our study begins with a specification of the mathematical form of the learning rules that we consider and a comparison between voltage-based rules and ordinary STDP (Section 2.1). Subsequently, we review benefits of time- and event-driven schemes for updating neurons and synapses, respectively (Section 2.2), and present two different algorithms for archiving histories of postsynaptic state variables (Section 2.3). In Section 2.4 we detail the reference implementation of the algorithms in NEST, and evaluate their performance in Section 3. There we discuss the Clopath rule (Section 3.1) and the Urbanczik-Senn rule (Section 3.2) in terms of implementation, reproduction of results from the literature and performance. Conclusions from the implementation of the two rules are drawn in Section 3.3, followed by a general Discussion in Section 4. The technology described in the present article will be made available with the next major releases of the simulation software NEST as open source. The conceptual and algorithmic work is a module in our long-term collaborative project to provide the technology for neural systems simulations (**Gewaltig and Diesmann**, 2007).

2 MATERIALS AND METHODS

2.1 Learning rules

The focus of this study are plasticity models of the general form

$$\frac{dW_{ij}(t)}{dt} = F(W_{ij}(t), s_i^*(t), s_j^*(t), V_i^*(t)) \tag{1}$$

where the change $\frac{dW_{ij}(t)}{dt}$ of the synaptic weight W_{ij} between the presynaptic neuron j and postsynaptic neuron i is given by a function F that potentially depends on the current synaptic weight $W_{ij}(t)$, as well as on $s_i^*(t), s_j^*(t), V_i^*(t)$ which are causal functionals of the postsynaptic spike train s_i, the presynaptic spike train s_j, and the postsynaptic membrane potential V_i, respectively (Figure 1). Note that for simplicity of the notation, we only show one function F on the right hand side of (1), while generally there could be a sum of multiple functions or functionals F_α, where each one depends on spike trains and membrane potentials in a different manner. Note also that F mixes information of pre- and postsynaptic neurons, while the functionals denoted by $*$ only need to take into account information of either the pre- or postsynaptic neuron. In cases where F is a functional, it can take into account an additional joint history dependence on s_i^*, s_j^* and V_i^*. A special case, the Urbanczik-Senn learning rule, is discussed in the results.

One can formally integrate (1) to obtain the weight change between two arbitrary time points t and T

$$\Delta W_{ij}(t, T) = \int_t^T dt' F(W_{ij}(t'), s_i^*(t'), s_j^*(t'), V_i^*(t')). \tag{2}$$

In general, the integral on the right hand side of the equation cannot be calculated analytically. There is, however, a notable exception, which is the model of spike-timing dependent plasticity (STDP). This model is a form of Hebbian plasticity that relies on the exact spike times of pre- and postsynaptic neurons and ignores any effect of the postsynaptic membrane potential. The dependence on the exact spike times becomes apparent by the fact that either the pre- or postsynaptic spike functional is the spike train itself, for example

$$s_i^*(t) = s_i(t) = \sum_k \delta(t - t_i^k), \tag{3}$$

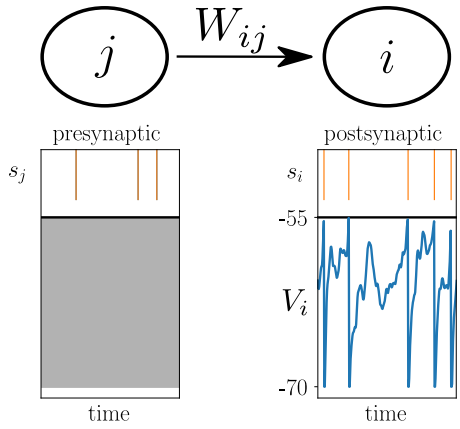

Figure 1. Voltage-based plasticity rules. The change ΔW_{ij} in synaptic strength between presynaptic neuron j and postsynaptic neuron i depends on the presynaptic spike train s_j,the postsynaptic spike train s_i and the postsynaptic membrane potential V_i.

where t_i^k is the k-th spike of the i-th neuron. This yields a plasticity rule that reads (**Morrison et al.**, 2008)

$$\frac{dW_{ij}(t)}{dt} = -f_-(W_{ij}(t))s^*_{-,i}(t)s_j(t) + f_+(W_{ij}(t))s^*_{+,j}(t)s_i(t) \tag{4}$$

with functions $f_\pm$ that model the weight dependence, and functionals $s^*_\pm(t) = (\kappa_\pm * s)(t)$ with exponential kernels $\kappa_\pm$. The appearance of the raw spike trains (delta distributions) in the differential equation of the STDP model renders the integration of the ODE trivial

$$\Delta W_{ij}(t,T) = -\sum_{\text{spikes } k} f_-(W_{ij}(t_j^k))s^*_{-,i}(t_j^k) + \sum_{\text{spikes } l} f_+(W_{ij}(t_i^l))s^*_{+,j}(t_i^l), \tag{5}$$

where $t_j^k, t_i^l \in [t,T]$. An update of the synaptic weight between any two time points only requires knowledge of the weight and spike functionals at the timing of the pre- and postsynaptic spikes.

For models that do not solely rely on exact spike times, but for example on filtered versions of the spike trains, much more information is needed in order to calculate a weight update $\Delta W_{ij}(t,T)$ between any two time points. This makes the computation more involved: the synapse needs all values of $W_{ij}(t'), s_i^*(t'), s_j^*(t'), V_i^*(t')$ for $t' \in [t,T]$ to update its weight. The remainder of this study describes different approaches to this problem and their advantages and disadvantages.

2.2 Time-driven vs event-driven update schemes

Modern neural network simulators have a modular code structure with individual objects for each synapse and neuron. Given this modularity, the question arises when in a simulation a specific part of the code needs to be executed. Spikes at individual synapses are rare (Figure 2A). Only at these points in time, the synaptic weight needs to be known as any weight dynamics in between two spikes is invisible to the rest of the network. This suggests to execute synapse code only when an actual event, i.e. a spike, is happening. The speedup that is achieved by this rare code execution gets evident by considering that each neuron can have up to thousands of synapses in cortical networks, which for large networks quickly becomes an immense amount of synapses in total. The large in-degree of individual neurons, however, changes the picture for neurons: They each receive a large amount of spikes in rapid succession (Figure 2B). This

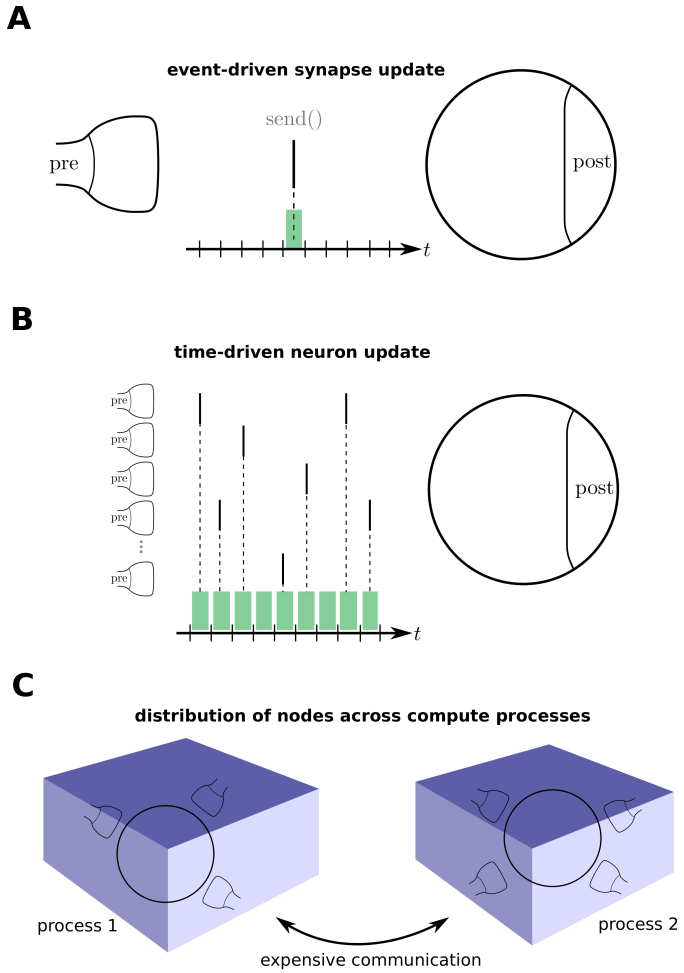

Figure 2. Update schemes for neurons and synapses. A A spike crosses a synapse from the presynaptic (pre) to the postsynaptic (post) neuron. Since this is a rare event, the synaptic weight is computed only when the `send()` function of the synapse is called (event-driven update). **B** Neurons with a large in-degree receive spikes in most of the time steps which suggests a time-driven update of the neuron's state. **C** Since the computation of the synaptic weights requires information from the postsynaptic neuron, storing the synapses on the same compute node reduces the amount of expensive communication between compute processes.

suggests a time-driven update of neurons. As a consequence, the membrane potential in many simulators is computed at each simulation step $t^\alpha = \alpha \cdot h$, where h is the simulation stepsize and $\alpha \in \mathbb{N}$. For plasticity models that rely on the membrane potential, the time discretization of (2) therefore yields

$$\Delta W_{ij}(t, T) = \sum_{\text{steps } \alpha} \Delta W_{ij}(t^\alpha, t^{\alpha+1}), \tag{6}$$

$$\Delta W_{ij}(t^\alpha, t^{\alpha+1}) = \int_{t^\alpha}^{t^{\alpha+1}} dt' F(W_{ij}(t'), s_i^*(t'), s_j^*(t'), V_i^*(t^\alpha)). \tag{7}$$

which, in comparison to the small sum over spikes in the STDP rule (5), contains a large sum over all time steps t^α in between time points t and T. Here, the membrane potential enters in a piecewise constant manner – hence the argument $V(t^\alpha)$. The synapse therefore predominantly needs information of the

	time-driven	event-driven	event-driven & compression
history length L	1	I	i
synapse function calls M	$K \cdot T$	$K \cdot T/I$	$K \cdot T/I$
weight change computations C	$K \cdot T$	$K \cdot T$	T
history entry manipulations H	T	T	$K \cdot T/I \cdot i$

Table 1. Comparison of synapse update schemes. From the view point of a postsynaptic neuron, the table shows the maximal length of the history L, the number of function calls M of synapse code, the number of computations C of infinitesimal weight changes $\Delta W_{ij}(t^\alpha, t^{\alpha+1})$, and the number of history entry manipulations H for a simulation of T time steps, a uniform inter-spike interval I between spikes of a single presynaptic neuron, and an in-degree K for each neuron and no delays. For the event-driven compression scheme the entries show the length of the compressed history where i is the number of different spike times within the last inter-spike interval I.

postsynaptic neuron in order to update its weight. Thus, in a distributed simulation framework, where neurons are split across multiple compute processes, it is beneficial to store the synapses at the site of the postsynaptic neurons in order to reduce communication (Figure 2C). This confirms the earlier design decision of **Morrison et al.** (2005) who place synapses at the site of the postsynaptic neuron to reduce the amount of data communicated by the presynaptic site.

If weight changes ΔW_{ij} depend on the synaptic weight themselves, then (7) cannot be used in practice as intermediate weights $W_{ij}(t')$ for $t^\alpha < t' < t^{\alpha+1}$ are not known. In this scenario, weight changes have to be calculated on the simulation grid with $W_{ij}(t') \to W_{ij}(t^\alpha)$ in case of a forward Euler scheme, or $W_{ij}(t') \to W_{ij}(t^{\alpha+1})$ in case of a backward Euler scheme. In the following we, for simplicity, stick to the forward Euler setting and arrive at the core computation for voltage-based plasticity rules

$$\Delta W_{ij}(t^\alpha, t^{\alpha+1}) = \int_{t^\alpha}^{t^{\alpha+1}} dt' F(W_{ij}(t^\alpha), s_i^*(t'), s_j^*(t'), V_i^*(t^\alpha)). \tag{8}$$

Given that s_i and s_j are spike trains, the functionals s_i^* and s_j^* are obtained trivially from their corresponding convolution kernels. If F in addition does not depend on s_i^* and s_j^* in a too complicated manner, which is usually the case (see examples in Section 3), the integral in (8) can be calculated analytically.

Let's assume in the following that t and T denote two consecutive spike times of the presynaptic neuron j. In this case, the synaptic weight corresponding to the spike at time T can be obtained from the weight $W_{ij}(t)$ at the time of the previous spike at t and (6) by employing (8) to calculate the latter. As F mixes information of the pre- and postsynaptic neurons, this computation should be done in the synapse. Since there are no spikes in between t and T, it does not matter when the synapse is performing the updates of its weight. Two possibilities are: 1) Neurons calculate their own s^* and V^* for the current time step and make it accessible to the synapse to enable direct readout and update according to (8) in every time step. This method corresponds to a time-driven update of synapses (Figure 3A). 2) Neurons store a history of s^* and V^* and the synapse reads out this information at T, i.e. at the time where the weight update becomes relevant for the network. This method corresponds to an event-driven update of synapses (Figure 3B). Both methods have their advantages and disadvantages analyzed in the following section.

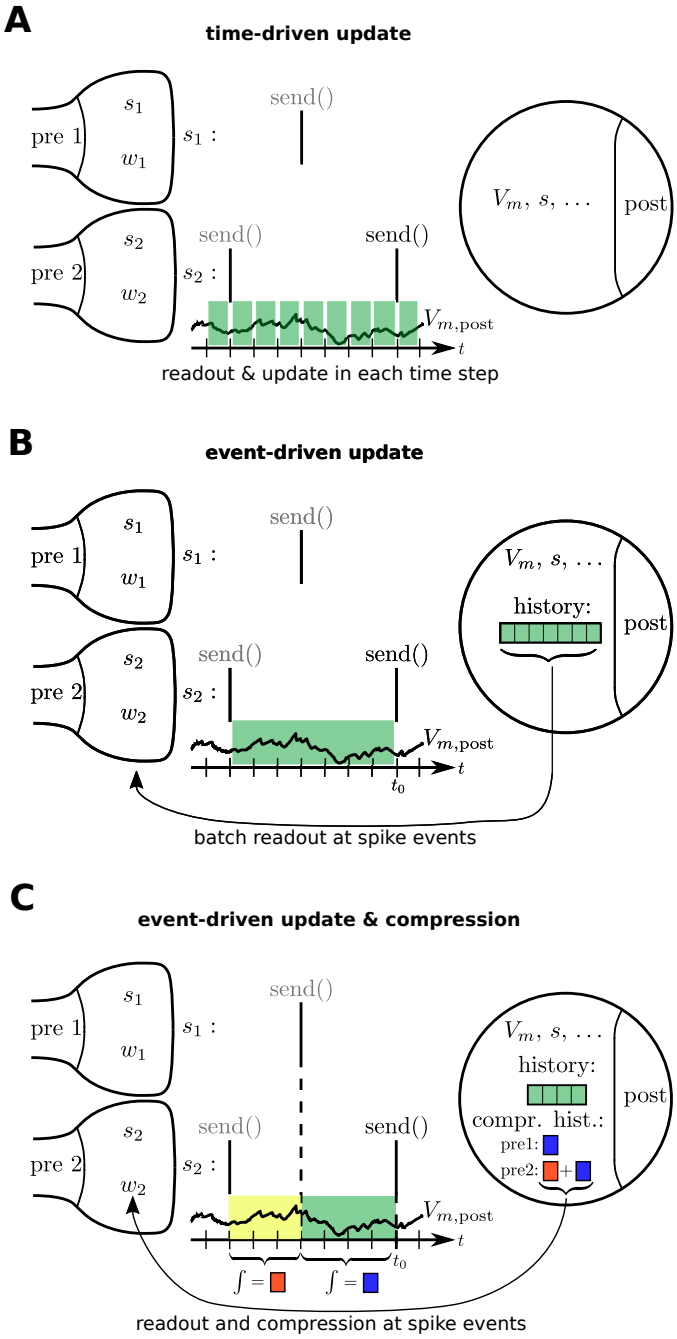

Figure 3. Simulation concepts. **A** In the time-driven update scheme the synaptic weight change is evaluated in every time step of the simulation for all the synapses. Thus, the postsynaptic quantities, e.g. the membrane potential $V_{m,\text{post}}$, are processed immediately. No storage of information is needed and the weight is always available if a spike is sent from a presynaptic (pre) to a postsynaptic (post) neuron using the `send()`-function of the synapse. **B** In the event-driven update scheme the computation of the synaptic weight change is performed only if a spike crosses the synapse. Therefore, the postsynaptic neuron needs to store the time trace of $V_{m,\text{post}}$ in a buffer (history, green). Whenever a spike is delivered, the new synaptic weight is computed inside the `send()`-function. To this end the synapse reads out the part of the history that corresponds to the period from its last spike to the current one. **C** In the compressed event-driven update scheme a synapse processes the history from the last spike that arrived at the postsynaptic neuron from any synapse to the current spike, e.g. from the first to the second (yellow) or from the second to the third (green). The result (red and blue, respectively) is used to update the weight changes of all synapses which are stored in a buffer called *compressed history*. After this operation, the active synapse reads out its weight change. Within this scheme the postsynaptic neuron needs to record $V_{m,\text{post}}$ from the time of the last incoming spike.

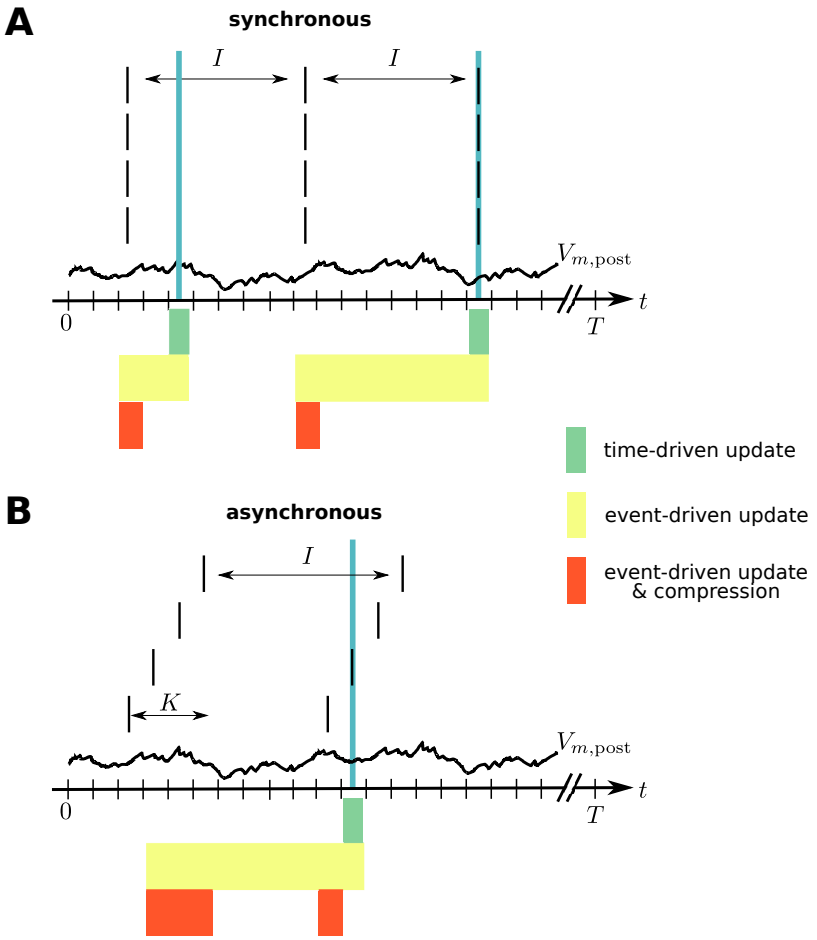

Figure 4. Illustration of buffer sizes for different simulation schemes in case of fully synchronous or asynchronous spikes. A All incoming spikes arrive synchronously: In the time-driven scheme the synaptic weight is updated in every time step of the simulation, so that only the current value of $V_{m,\mathrm{post}}$ needs to be available (green). In the event-driven scheme every synapse processes $V_{m,\mathrm{post}}$ from the last spike to the current one. Therefore, the relevant time trace needs to be stored (yellow). In the compressed event-driven scheme this part of $V_{m,\mathrm{post}}$ is processed only once and used to update the weight of all the synapses. Since the weight change is a function of the last spike time which is the same for all the synapses, only one value needs to be updated (red). In this situation the length L of the compressed history is $i = 1$, see Table 1. **B** All incoming spikes arrive in different time bins: For the time-driven and the event-driven scheme the scenario is similar to panel A. For the compressed event-driven scheme the number of values that need to be updated equals the number of incoming synapses K so that $i = K$.

2.3 Simulation concepts

2.3.1 Time-driven scheme

An event-based update of synapses requires each neuron to store its membrane potential at the resolution of the simulation time step. This amounts to an increase in memory consumption as opposed to simulations without voltage-based plasticity. A time-driven update circumvents this problem as the information on the membrane potential is directly processed by the synapses such that only the current value of the membrane potential needs to be stored, corresponding to a membrane potential history of length $L = 1$ (Figure 4 and Table 1). The price for this is that synapses need to be updated as often as neurons. For a simulation of T time steps this amounts to $M = K \cdot T$ function calls to synapse code for each neuron. Here K denotes the in-degree, i.e. the number of incoming connections per neuron. Each function call of synapse

code causes a single computation of $\Delta W_{ij}(t^\alpha, t^{\alpha+1})$, giving rise to in total $C = K \cdot T$ computations per neuron. The membrane potential trace is thus effectively integrated K times; once for each synapse. As both K and T are large numbers in typical simulations of plastic cortical networks, the amount of function calls and computations is therefore large in this setting. Another disadvantage is that the synapse is being updated also at time steps, where s_i^*, s_j^*, V_i^* have values for which $\Delta W_{ij}(t^\alpha, t^{\alpha+1}) = 0$ vanishes, i.e. where no update is required. In addition, for delayed connections a history of V_i^* of length $L = d_{\max}$ of the maximal delay $d_{\max}$ measured in simulation steps needs to be stored. We here assume the delay to be on the postsynaptic side; it represents the time the fluctuations of the somatic membrane potential propagate back through the dendrites to the synapses. Therefore, F does not depend on $V_i^*(t)$, but on $V_i^*(t - d_j)$ with a delay d_j encoding the location of the synapse with presynaptic neuron j.

2.3.2 Event-driven scheme

In an event-driven update scheme of synapses, the time trace of the membrane potential V_i^* needs to be stored until all presynaptic synapses have read out the information to update their weight for a given period. The storage and management of such a history can be expensive in terms of memory and runtime. Assuming for simplicity a homogeneous inter-spike interval of I time steps between consecutive spikes of single neurons, we in the following showcase some qualitative history sizes. As synapses need all values of V_i^* in between two consecutive spikes, the maximum history length is $L = I$ (Figure 4). In case of different firing rates, I corresponds to the maximum inter-spike interval of any of the presynaptic neurons. Synapse code in this scheme is, however, only called in the event of a spike, leading to only $M = K \cdot T/I$ function calls per neuron, where T/I is the number of spikes passing a single synapse during simulation time T. The total amount of computations C of weight changes $\Delta W_{ij}(t^\alpha, t^{\alpha+1})$ is of course unchanged with respect to the time-driven scheme; they are just split across less function calls ($C = M \cdot L = K \cdot T$). Table 1 immediately shows the trade-off between memory consumption (length of history) and run time (number of function calls): the event-based scheme consumes more memory, but is faster than the time-driven scheme. Note that since a history of the membrane potential is stored anyway, this scheme is naturally applicable to connections with different delays. A further performance increase can be achieved in plasticity rules, where weight changes only happen under certain conditions on V_i^*: if values $\Delta W_{ij}(t^\alpha, t^{\alpha+1}) \neq 0$ are rare, a non-continuous history can be stored. In such a scenario, time stamps need to be stored alongside the membrane potential to enable synapses to read out the correct time intervals (see Section 3.1).

2.3.3 Data compression

The major operation of the plasticity scheme in terms of frequency and complexity is the computation of infinitesimal weight changes $\Delta W_{ij}(t^\alpha, t^{\alpha+1})$. Since the presynaptic spike train s_j^* enters F in (8), the same postsynaptic information on s_i^* and V_i^* is used many times for very similar computations: the membrane potential trace of each neuron is effectively integrated K times. Is there a way to employ the result of the computation $\Delta W_{ij}(t^\alpha, t^{\alpha+1})$ for neuron j for the computations $\Delta W_{ik}(t^\alpha, t^{\alpha+1})$ for other neurons $k \neq j$? In a simple setting, where F factorizes into $F(W_{ij}(t), s_i^*(t), s_j^*(t), V_i^*(t)) = s_j^*(t)\, G\left(s_i^*(t), V_i^*(t)\right)$ with $s_j^*(t) = (\kappa * s_j)(t)$ and

$$\kappa(t) = H(t)\, \frac{1}{\tau} e^{-\frac{t}{\tau}}, \tag{9}$$

defined via the Heaviside step function $H(x)$, we can make use of the property

$$s_j^*(t) = \left(s_j^*(t_{LS}) + \tau^{-1}\right) e^{-(t - t_{LS})/\tau}, \tag{10}$$

where $t > t_{LS}$ and t_{LS} denotes the last spike time of the presynaptic neuron. In this case the weight update factorizes

$$\Delta W_{ij}(t_{LS}, T) = \underbrace{(s_j^*(t_{LS}) + 1)}_{=:\bar{x}_j(t_{LS})} \underbrace{\int_{t_{LS}}^{T} dt' e^{-(t'-t_{LS})/\tau}\, G(s_i^*(t'), V_i^*(t'))}_{=:\Delta W_i(t_{LS},T)} \tag{11}$$

where the latter factor $\Delta W_i(t_{LS}, T)$ is independent of the presynaptic spike train s_j^*. This opens the possibility to directly compute and store $\Delta W_i(t_{LS}, T)$ at the postsynaptic neuron i. The advantage is that the integration in (11) only needs to be performed once. At the time of an incoming spike event, $\Delta W_i(t_{LS}, T)$ can be read out by the synapse for the correct t_{LS} of that synapse and combined with the stored presynaptic spike trace $\bar{x}_j(t_{LS})$.

This scheme a priori amounts to the same number of function calls to synapse code ($M = K \cdot T/I$) and the same maximum history length ($L = I$) as in the ordinary event-driven scheme. For each time step $\Delta W_i(t^\alpha, t^{\alpha+1})$ is computed once in the neuron rather than in the synapse, but its value is used to update all entries in the history $\Delta W_i(t_{LS}, T)$. The latter operation is costly, as the history is potentially long ($L = I$). This can be improved by noting that $\Delta W_i(t_{LS}, T)$ does not need to be stored for all $t_{LS} \in [T - I, T]$, but only for those times, where presynaptic neurons fired: For in-degree $K < I$ or synchronous spiking, the number of time bins with spikes can be much lower than I (Figure 4). Storing only relevant $\Delta W_i(t_{LS}, T)$ therefore requires knowledge of the postsynaptic neurons on the last spike times of all its presynaptic neurons.

The time-driven update of the history can be avoided by updating the history $\Delta W_i(t_{LS}, T)$ in an event-driven manner (Figure 3C): In between any two incoming spikes T_1 and T_2, the postsynaptic neurons stores $V_i^*(t)$. At the time T_2 of the new spike, the stored $V_i^*(t)$ is read out and integrated for the range $[T_1, T_2)$

$$\delta W_i(T_1, T_2) = \int_{T_1}^{T_2} dt' e^{-t'/\tau} G(s_i^*(t'), V_i^*(t')) \tag{12}$$

such that all entries in the history $\Delta W_i(t_{LS}, T)$ can be updated as $\Delta W_i(t_{LS}, T_2) = \Delta W_i(t_{LS}, T_1) + e^{t_{LS}/\tau}\, \delta W_i(T_1, T_2)$. To avoid too large or small arguments of exponentials in numerical implementations, one equivalently calculates

$$\delta \mathcal{W}_i(T_1, T_2) = \int_0^{T_2 - T_1} dt'\, e^{-t'/\tau}\, G(s_i^*(t' + T_1), V_i^*(t' + T_1))$$

such that $\delta W_i(T_1, T_2) = e^{-T_1/\tau} \delta \mathcal{W}_i(T_1, T_2)$ and $\Delta W_i(t_{LS}, T_2) = \Delta W_i(t_{LS}, T_1) + e^{-(T_1 - t_{LS})/\tau} \delta \mathcal{W}_i(T_1, T_2)$. Afterwards the history of $V_i^*(t)$ is deleted. This way the latter history is always short as the total rate of incoming spikes is high in physiological network states.

This event-driven compression amounts to a compressed history of length $L = i$, where i is the number of different spike times within the last inter-spike interval I. It is consequently never larger than the history length $L = I$ of the ordinary event-driven scheme. Still, synapse code is executed at every spike event, giving rise to $M = K \cdot T/I$ function calls. For synchronous spikes, the history, however, only needs to be updated once. The membrane potential trace is therefore effectively only integrated once, amounting to $C = T$ infinitesimal weight change computations (Table 1). The price for this is that history updates are more expensive: instead of appending a single entry in each time step, at each spike event the full history

is updated, giving rise to in total $H = K \cdot T/I \cdot i$ history entry manipulations, as opposed to $H = T$ in time- and ordinary event-driven scheme Table 1. In practice, infinitesimal weight change computations are, however, often more costly than history updates, such that there is a performance increase achieved by the compression algorithm (see Section 3.2).

Finally, a drawback of the event-driven compression is that it relies on the fact that all synapses use the same processed membrane potential V_i^*. For distributed delays, $\Delta W_i(t_{LS}, T)$ has a dependence on the presynaptic neuron j via $V_i^*(t - d_j)$. In this case, a separate compressed history needs to be stored for every different delay of connections to the neuron.

The considerations above illustrate conceptual differences in the different schemes rather than quantitative bounds for efficiency. The remainder of the work describes reference implementations of the three schemes and examines their performance for two example plasticity rules from the literature.

2.4 Reference implementation in network simulator with event-based synapse updates

This section describes the implementation of two example voltage-based plasticity rules by **Clopath et al.** (2010) and **Urbanczik and Senn** (2014) in a spiking neural network simulator that employs a time-driven update of neurons and an event-based update of synapses. While the naming conventions refer to our reference implementation in the simulation software NEST, the algorithms and concepts presented below are portable to other parallel spiking network simulators.

The Clopath and Urbanczik-Senn rule are chosen as widely used prototypical models of voltage-based plasticity. The differences in the two rules help to exemplify the advantages and disadvantages of the algorithms discussed in Section 2.3. As originally proposed, they are implemented here for two different types of neuron models, Ad-ex/Hodgkin-Huxley point-neurons for the Clopath rule (`aeif_psc_delta_clopath`/`hh_psc_alpha_clopath`) and two-compartment Poisson neurons (`pp_cond_exp_mc_urbanczik`) for the Urbanczik-Senn rule. The rules differ in the state variable that is being stored and its interpretation. For the Clopath rule, the stored variable is a thresholded and filtered version of the membrane potential that takes into account characteristics of membrane potential evolution within cells in the vicinity of spike events. The latter restriction to temporal periods around spikes suggests to implement a history that is non-continuous in time. In contrast, the Urbanzcik-Senn rule uses the dendritic membrane potential to predict the somatic spiking; the resulting difference is taken as an error signal that drives learning. This error signal never vanishes and thus needs to be stored in a time-continuous history.

Finally, the proposed infrastructure for storing both continuous and non-continuous histories is generic so that it can also be used and extended to store other types of signals such as external teacher signals. Details on the Clopath and Urbanczik-Senn rule are discussed in Section 3.

2.4.1 Exchange of information between neurons and synapses

The implementation of voltage-based plasticity rules in NEST follows the modular structure of NEST, key part of which is the separation between neuron and synapse models. This separation makes it easy for a newly added neuron model to be compatible with existing synapse models and vice versa. A downside is that information, such as values of parameters and state variables, is encapsulated within the respective objects. Simulations in NEST employ a hybrid parallelization scheme: OpenMP threads are used for intra node parallelization and the Message Passing Interface (MPI) for inter node communication. In parallel simulations, synapses are located at the same MPI process as the postsynaptic neurons (**Morrison et al.**, 2005). Thereby, no communication between MPI processes is needed for the required transfer of

information between postsynaptic neurons and synapses to compute weight changes of connections and only one spike needs to be communicated by a given source neuron for all target neurons living on the same MPI process.

The model of STDP requires synapses to access spike times of postsynaptic neurons. In order to provide a standardized transfer of this information across all neuron models that support STDP, in recent years the so-called `Archiving_Node` has been introduced as a parent class of the respective neuron models (**Morrison et al.**, 2007a). It provides member functions to store and access spike histories. If a neuron model supports STDP, it only needs to be a child of `Archiving_Node` and contain one additional line of code, namely a call of the function `set_spiketime()`, which stores the time of outgoing spike events. We here extended this framework for voltage-based plasticity rules and enhanced the functionality of the archiving node by the member functions `write_history()` and `get_history()` to additionally store voltage traces or other continuous signals. To avoid overhead for simulations with only STDP synapses, we introduced two child classes of `Archiving_Node`, `Clopath_Archiving_Node` and `Urbanczik_Archiving_Node`, that each provide containers and functions for the specific histories required for the two plasticity rules. Neuron models that support the respective synapse model then derive from the child classes instead of the root level archiving node.

One complication arises if the calculation of the processed membrane potential V^* inside the archiving node requires parameters or functions that are specific to the neuron model. One example is the gain function ϕ that translates the membrane potential into a firing rate in case of the Poisson neuron model used in **Urbanczik and Senn** (2014) and here to demonstrate the Urbanczik-Senn rule: ϕ as well as its parameters have to be specified for the neuron, but they also enter the plasticity rule through V^*. Creating an additional helper class (`pp_urbanczik_parameters`) as a template argument for the corresponding archiving node (`Urbanczik_Archiving_Node`) and neuron model (`pp_cond_exp_mc_urbanczik`) solves this problem (Figure 5): it contains all parameters and functions required by both classes.

2.4.2 Update schemes

All synapses implemented in NEST are so far purely event-driven. To assess the performance of the time-driven update scheme of synapses with voltage-based plasticity, we also implemented a time-driven version of the Clopath and Urbanczik-Senn synapse. Spiking network simulators exploit the delay of connections to reduce communication between compute processes: for the period of the minimal delay, neurons are decoupled and state variables can be propagated forward in time independent of each other. Spikes are therefore buffered and sent at the end of a `min_delay` period, and neuronal updates are batched for all time steps within one `min_delay`. We implemented the same `min_delay` update scheme for synapses, by imposing a function call to time-driven synapses in every `min_delay` period to update their synaptic weight. If `min_delay` equals the simulation step size h, this scheme corresponds to the scheme explained in Section 2.3.1. Making use of the `min_delay` infrastructure in NEST speeds up simulations with time-driven synapses in the case $d > h$ as fewer function calls to synapses are needed (see Section 3). In case of simulations with synaptic delays, the time-driven update scheme requires the storage of a history of the membrane potential of length `max_delay`.

Storing state variables in event-driven schemes is more complex as the history does not have a fixed length `max_delay`. Instead it needs to be dynamically extended and shortened. A long history can occupy a large amount of memory and its processing by the synapses becomes computationally expensive. Therefore, it is advantageous to optimize the way how information is stored and accessed and how entries that are no longer needed can be identified for deletion.

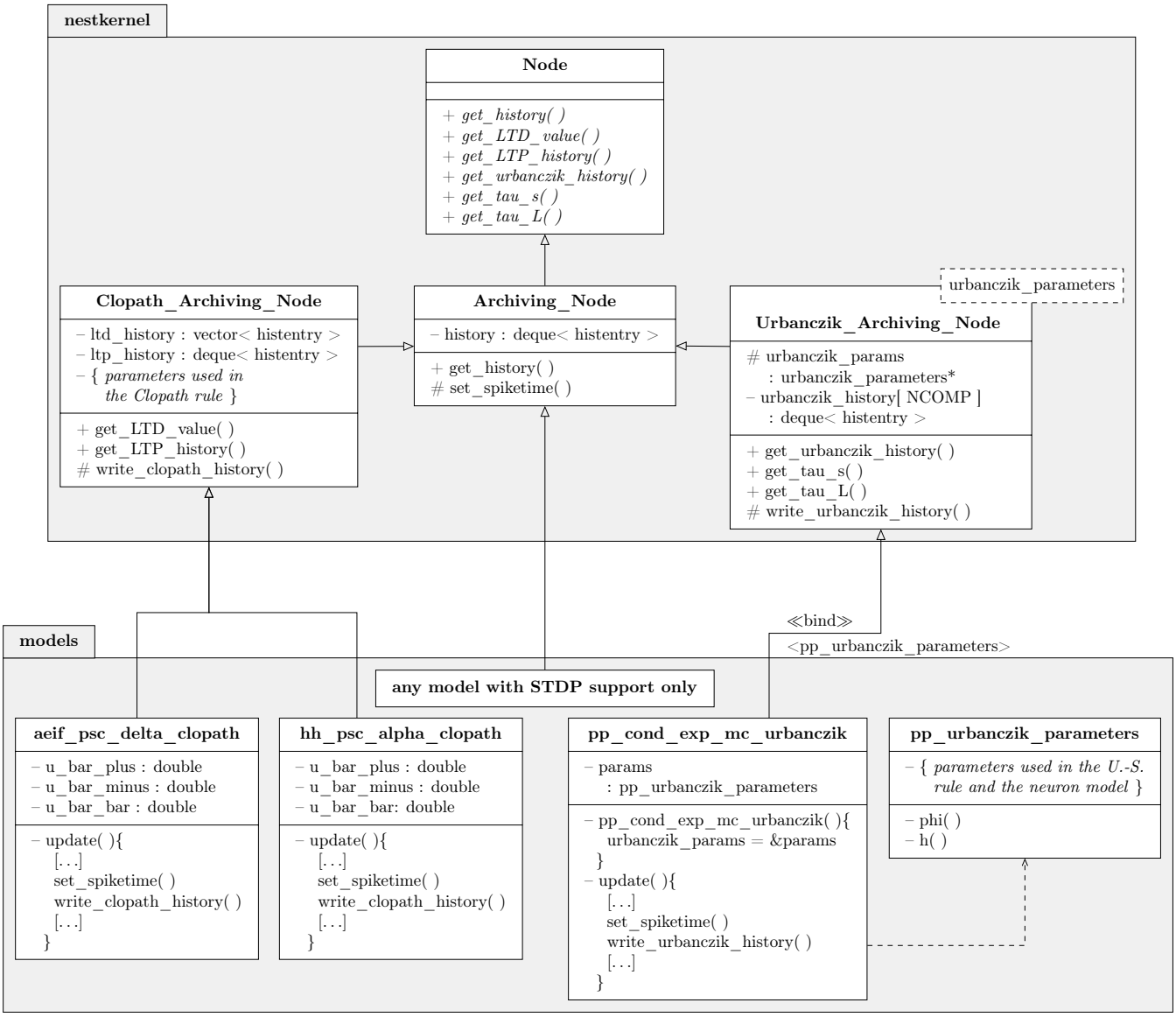

Figure 5. Class diagram of NEST classes and functions. Simplified class diagram for embedding the Clopath (left) and Urbanczik-Senn rule (right) in the NEST infrastructure. The code is distributed across the `nestkernel` and neuron models. `nestkernel` contains the base class `Node` of all neurons models. Models that support ordinary STDP are derived from the `Archiving_Node`, models that can use the Clopath synapse (`aeif_psc_delta_clopath` and `hh_psc_alpha_clopath`) or Urbanczik-Senn synapse (`pp_cond_exp_mc_urbanczik`) are derived from the `Clopath_Archiving_Node` or the `Urbanczik_Archiving_Node`, respectively. The latter add the required functions for storing and managing the history of continuous quantities. The model `pp_cond_exp_mc_urbanczik` requires a helping class `pp_urbanczik_parameters` because the `Urbanczik_Archiving_Node` needs to access functions and parameters that are specific to the neuron model and therefore not located in the `Urbanczik_Archiving_Node` to keep its implementation more general.

2.4.3 History management

There are three points that need to be considered in the context of history management: Firstly, which information needs to be stored. Secondly, how to search and read out the history. Thirdly, how to identify and remove information that is no longer needed. The first and third point mainly affect memory usage, the second the simulation time as searching in shorter histories is faster.

There are four different histories to which our considerations apply. The one to store the membrane potential V_i^*, the compressed history $\Delta W_i(t_{LS}, T)$ used only for the compressed event-driven scheme, the history to store the spike times s_i of the postsynaptic neuron (also used for ordinary STDP), and finally one might need a history that stores the last spike time for every incoming synapse (see below for details).

2.4.3.1 Adding information to the history:

This paragraph concerns only the history that stores the time trace of V_i^*. In every time step of the simulation, neurons call the protected function `write_history()` of the archiving node and pass the current value of the (low-pass filtered) membrane potential. The archiving node then computes the derived quantities V_i^* and potentially combinations of V_i^* and s_i^*, and saves them in the history, which is of type `vector`. It is more efficient to do the computations inside the archiving node and not in the synapse for two reasons: Firstly, the computation is done once for all incoming synapses and secondly, if the number of derived quantities is smaller than those of the bare quantities, less memory is used to store the history.

2.4.3.2 Readout of information from the history:

Let us assume that a synapse requests a part from t_1 to $t_2 > t_1$ of the history that ranges from $t_{\text{start}} < t_1$ to $t_{\text{end}} > t_2$. In case every time step of the simulation adds a new entry to the history, one can easily compute the positions of the entries corresponding to $t_{1/2}$ by just knowing t_{start} and t_{end}. We will learn in Section 3.2 that this is the case for the Urbanczik-Senn plasticity rule. If the history is not continuous in time, like in case of the Clopath rule, this scheme is not applicable. Instead, we add a time stamp s as an additional variable to each entry and search for those with the smallest/greatest s within the interval (t_1, t_2) using e.g. a linear or a binary search. Searching for the positions that define the start and the end of the requested interval is slower than computing them directly. Nevertheless, a non-continuous history can be advantageous as we will see in case of the Clopath rule (Section 3.1). Here, only values of the membrane potential in the vicinity of a spike of the postsynaptic neuron are needed so that neglecting the majority of values in between leads to a non-continuous history but saves memory.

Technically, the archiving node contains a function called `get_history()` which expects two iterators `start` and `finish` and two times t_1 and t_2. When executed, the function sets the iterators to point to the entries corresponding to t_1 and t_2, respectively. In the event-driven scheme this is used by the synapse which provides the time of the last spike $t_1 = t_{\text{LS}} - d$ and that of the current spike $t_2 = t_{\text{S}} - d$, to set two pointers to the correct position of the history of the postsynaptic neuron. Here, d accounts for the delay, the information of the postsynaptic neuron is shifted by d backwards in time at the synapse. Having received the correct position of the pointers, the synapse evaluates the integral (6). In the event-driven compression scheme, the integration (12) is not done inside the synapse but inside the `archiving_node`. The reason for this is that the compressed history $\Delta W_i(t_{LS}, T)$, which is updated in case of an incoming spike, is stored inside the `archiving_node`. This way no exchange of information is needed. The synapse only triggers the updating process by calling the function `compress_history()` of the `archiving_node`. Internally, the `archiving_node` can use `get_history()` to obtain the part of the history that has to be integrated. Even though the linear search a priori might seem less efficient than a binary search or direct computation of the position, it turns out that it has an advantage in that it iterates consecutively over the history entries which can be employed to identify data no longer needed. Therefore, especially for short histories a simple iteration that comes without any overhead is fastest (see Section 3.1).

2.4.3.3 Removing information from the history:

To prevent the history from occupying an unnecessary amount of memory, it is crucial to have a mechanism to delete those entries that have been used by all incoming synapses. The simplest implementation to identify these entries is to add one additional variable to each entry called *access counter* initialized to zero when the entry is created. When a synapse requests a part from t_1 to t_2 of the history, the algorithm iterates over all entries $t_1 < t < t_2$ and increases the access counters by one. After the update of the synaptic weight all entries whose access counters are equal to the number of incoming synapses are deleted. This scheme can be combined easily with a linear search starting the iteration from the oldest entry of the history.

For long histories a linear search is inefficient and should be replaced by a binary search or direct computation of positions if applicable. To avoid iteration within long histories, we replace access counters by a vector that stores the last spike time t_{LS} for every incoming synapse. If a synapse delivers a spike, it updates its entry in that vector by replacing t_{LS} by the time stamp of the current spike. After each weight update, searching the vector for the smallest t_{LS} allows us to safely remove all membrane potentials with time stamps $t < \min(\{t_{\mathrm{LS},i}\})$. In practice, we can further improve this mechanism with two technical details. Firstly, n incoming spikes with the same time stamp can share the same entry t_{LS} which we then have to provide with a counter that goes down from n to zero in steps of one whenever one of the n synapses sends a new spike for a time $t > t_{LS}$. Secondly, we can avoid the search for the smallest t_{LS} by making sure that the entries t_{LS} are in chronological order. This can be easily achieved if a synapse does not update its entry in the vector but removes it and appends a new one at the end of the vector.

2.4.4 Event-based compression scheme in NEST

As discussed in Section 2.3.3, the event-based compression scheme relies on the fact that all synapses to one postsynaptic neuron employ the same V_i^*. This is not the case if delays of the corresponding connections are distributed. The compression scheme can therefore only be efficient if all delays have a fixed value. If spikes are processed and synapses are updated in a chronological order, then a well-defined segment of the history of V_i^* can be integrated and the compressed history can be updated. In NEST, spikes are, however, buffered within a period of `min_delay` before being sent and processed. Consequently, synapses are not updated in chronological order. Therefore, the event-based compression scheme can only be implemented in NEST in the case where delays equal the simulation time step.

3 RESULTS

In the following, we evaluate the different simulation concepts of Figure 2 for the Clopath rule (**Clopath et al.**, 2010) and the Urbanczik-Senn rule (**Urbanczik and Senn**, 2014) and our reference implementation in the spiking network simulator NEST (**Jordan et al.**, 2019). For each of the voltage-based plasticity rules, we first detail the rule itself and discuss specificities of its implementations, before assessing their performance on a distributed computing architecture.

3.1 Clopath plasticity

The Clopath rule (**Clopath et al.**, 2010) was designed as a voltage-based STDP rule that accounts for nonlinear effects of spike frequency on weight changes which had been previously observed in experiments (**Sjöström et al.**, 2001). It does so by using the evolution of the postsynaptic membrane voltage around postsynaptic spike events instead of the postsynaptic spikes themselves. This requires a neuron model that takes into account features of membrane potential excursions near spike events, such as modified adaptive

exponential integrate-and-fire (aeif) model neurons that are used in the original publication (**Clopath et al.** (2010), see Section 5.1) or Hodgkin-Huxley (hh) neurons that are used in a reference implementation by B. Torben-Nielson on ModelDB (**Hines et al.**, 2004).

The plasticity rule is of the general form (1) with a sum of two different functions F_α on the right hand side. It treats long-term depression (LTD) and potentiation (LTP) of the synaptic weight in the two terms F_{LTD} and F_{LTP}, with

$$\begin{aligned} F_{\text{LTD}}\left(s_j(t), V^*_{i,\text{LTD}}(t)\right) &= -A_{\text{LTD}}\; s_j(t)\, V^*_{i,\text{LTD}}(t) \\ \text{with}\;\; V^*_{i,\text{LTD}} &= (\bar{u}_- \,-\, \theta_-)_+\,, \\ \bar{u}_-(t) &= (\kappa_- * V_i)(t - d_s) \end{aligned} \tag{13}$$

and

$$\begin{aligned} F_{\text{LTP}}\left(s^*_j(t), V^*_{i,\text{LTP}}(t)\right) &= A_{\text{LTP}}\; s^*_j(t)\, V^*_{i,\text{LTP}}(t) \\ \text{with}\quad s^*_j &= \kappa_s * s_j\,, \\ V^*_{i,\text{LTP}} &= (\bar{u}_+ \,-\, \theta_-)_+(V_i \,-\, \theta_+)_+\,, \\ \bar{u}_+(t) &= (\kappa_+ * V_i)(t - d_s)\,. \end{aligned} \tag{14}$$

Here $(x - x_0)_+ = H(x - x_0)\,(x - x_0)$ is the threshold-linear function and $H\,(x)$ is the Heaviside step function. A_{LTD} and A_{LTP} are prefactors controlling the relative strength of the two contributions. $\kappa_\pm$ are exponential kernels of the form (9), which are applied to the postsynaptic membrane potential, and κ_s is an exponential kernel applied to the presynaptic spike train. The time-independent parameters $\theta_\pm$ serve as thresholds below which the (low-pass filtered) membrane potential does not cause any weight change (Figure 6). Note that A_{LTP} can also depend on the membrane potential. This case is described in Appendix Section 5.3.

In a reference implementation of the Clopath rule by C. Clopath and B. Torben-Nielsen available on ModelDB (**Hines et al.**, 2004), there is a subtle detail not explicitly addressed in the original journal article. In their implementation the authors introduce an additional delay d_s between the convolved version of the membrane potentials $\bar{u}_\pm$ and the bare one (cf. parameter d_s in (13) and (14)). The convolved potentials are shifted backwards in time by the duration of a spike d_s (see Table 2 and Table 4). As a result, the detailed shape of the excursion of the membrane potential during a spike of the postsynaptic neuron does not affect the LTP directly but only indirectly via the low-pass filtered version $\bar{u}_+$, see green background in Figure 6B. Incorporating this time shift in $\bar{u}_\pm$ is essential to reproduce the results from **Clopath et al.** (2010) on spike-pairing experiments (Figure 7A,B).

The depression term F_{LTD} depends on the unfiltered spike train s_j. It can thus be treated analogous to ordinary STDP rules (cf. (4)ff). In particular, $V^*_{i,\text{LTD}}$ only needs to be available for time points of presynaptic spikes (potentially taking into account additional delays of the connection). The potentiation term F_{LTP}, however, depends on the filtered spike train s^*_j; $V^*_{i,\text{LTP}}$ consequently needs to be stored also for times in between spike events.

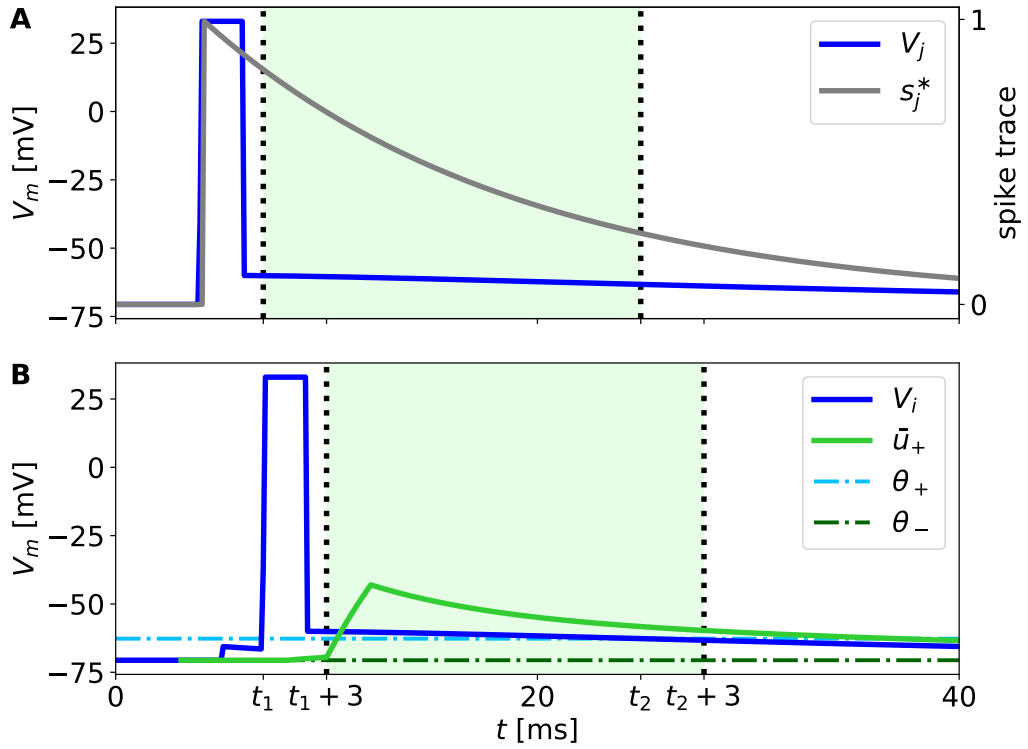

Figure 6. Illustration of LTP contribution to the Clopath rule. A presynaptic neuron (panel **A**) and a postsynaptic neuron (panel **B**) emit a spike at $t_{\text{sp,pre}} = 4\,\text{ms}$ and $t_{\text{sp,post}} = 6\,\text{ms}$, respectively. The presynaptic spike elicits a trace s_j^* (gray) at the synapse. The excursion of the postsynaptic membrane potential V_i (panel B, blue) elevates the low-pass filtered potential $\bar{u}_+$ (green) so that both V_i and $\bar{u}_+$ exceed the respective thresholds θ_+ (dash-dotted, dark blue) and θ_- (dash-dotted, dark green), cf. (14), between t_1 and t_2. Only within this period, shifted by $d_s = 3\,\text{ms}$, which is for times $t_1 + 3\,\text{ms} < t < t_2 + 3\,\text{ms}$ (panel B, green background), see Section 3.1.1 for details, the LTP of the synaptic weight is non-vanishing because of the threshold-linear functions in 14. The shift by $d_s = 3\,\text{ms}$ does not apply to the spike trace (panel A, green background). The rectangular shape of the spikes is achieved by a clamping of the membrane potential to $V_{\text{clamp}} = 33\,\text{mV}$ for a period of $t_{\text{clamp}} = 2\,\text{ms}$.

3.1.1 Implementation details of the Clopath rule

We implement both an adaptive exponential integrate-and-fire neuron model (`aeif_psc_delta_clopath`) and a Hodgkin-Huxley neuron model (`hh_psc_alpha_clopath`) supporting Clopath plasticity. Our implementation of `aeif_psc_delta_clopath` follows the reference implementation on ModelDB which introduced a clamping of the membrane potential after crossing the spiking threshold to mimic an action potential. Details can be found in Section 5.1. The implementations of `aeif_psc_delta_clopath` and `hh_psc_alpha_clopath` consider the filtered versions $\bar{u}_\pm$ of the membrane potential as additional state variables of the neuron. Thereby, they can be included in the differential equation solver of the neurons to compute their temporal evolution. Parameters of $\kappa_\pm$ consequently need to be parameters of the neuron rather than the synapse. The same is true for the values of $\theta_\pm$; they are used in the neuron to determine whether $V^*_{i,\text{LTP}}$ and $V^*_{i,\text{LTD}}$ evaluate to zero, which happens for many time steps due to the Heaviside functions in their definitions.

The LTD mechanism is convenient to implement within the event-driven framework: when the synapse is updated at time t, it reads the values $\bar{u}_-\,(t-d)$ and θ_- from its target and computes the new weight. Here,

d denotes the dendritic delay of the connection that accounts for the time it takes to propagate somatic membrane potential fluctuations to the synapse. The archiving node contains a ring buffer that stores the history of $\bar{u}_-$ for the past `max_delay` time steps so that the synapse can access a past value of this quantity. Consequently, the LTD history is always short and can be forgotten in a deterministic fashion.

The computation of the weight change due to LTP requires the evaluation of the integral over $V^*_{i,\mathrm{LTP}}(t)$. The latter is stored in the archiving node as a vector whose elements are objects that contain three values: the corresponding time t, the value of $V^*_{i,\mathrm{LTP}}$ and an access counter that initially is set to zero.

3.1.1.1 Time-driven update:

For simulations with delay equal to the simulation time step, the history of $V^*_{i,\mathrm{LTP}}$ always contains only a single value as it is read out in every time step by all synapses. For larger delays, the history is of length `max_delay`, and each synapse reads out a segment of length `min_delay`, increasing the access counter of the corresponding entries by one. For the last synapse that requests a certain segment, the access counter then equals the in-degree K, which is the criterion to delete the corresponding entries from the history. Although for simplicity done in our reference implementation, the time-driven scheme does not require us to store the time stamp t of each history entry. The overhead of this additional number is, however, negligible.

3.1.1.2 Event-driven update:

In event-driven schemes, the history of $V^*_{i,\mathrm{LTP}}$ dynamically grows and shrinks depending on the spikes of presynaptic neurons. Since many values of $V^*_{i,\mathrm{LTP}}$ are zero, it is beneficial to only store the non-zero values. In this case, a time stamp of each entry is required to assign values of the non-continuous history of $V^*_{i,\mathrm{LTP}}$ to their correct times. When a synapse j is updated at time t_S of a spike, it requests the part of the history between the last spike t_{LS} and the current spike t_S (minus the dendritic delay) from the archiving node. In case of the uncompressed scheme, t_{LS} thereby refers to the last spike of the same synapse j. This history segment is then integrated in synapse j and used for the update of synapse j. Each synapse thus integrates the history $V^*_{i,\mathrm{LTP}}$ anew (Section 2.3.2). For the compressed scheme, t_{LS} refers to the last spike of any synapse to neuron i. In this case, the history is integrated in the archiving node, the weight of synapse j is updated, and the compressed history for all other last spike times is updated. Afterwards the history of $V^*_{i,\mathrm{LTP}}$ is deleted. Thereby, $V^*_{i,\mathrm{LTP}}$ is only integrated once for all synapses.

In any case, the integrated history of $V^*_{i,\mathrm{LTP}}$ needs to be combined with the presynaptic spike trace s^*_i. The latter is easily computed analytically inside the synapse because it is an exponential decay of the corresponding value at the time of the last spike. At the end of the update process the trace is increased by τ_s^{-1} to account for the trace of the current spike, where τ_s is the time constant of the kernel κ_s.

The reference implementation reproduces the results from **Clopath et al.** (2010) on spike-pairing experiments and the emergence of bidirectional connections in orientation-selective networks (Figure 7). See Appendix Section 5.2 for details on the setup of both experiments as implemented in NEST.

3.1.2 Performance of the reference implementation

In order to evaluate the performance of the implementation of the Clopath rule in NEST, in a weak-scaling setup, we simulate excitatory-inhibitory networks of increasing size, but fixed in-degree K. As we expect the performance to critically depend on the number of synapses, we examine two scenarios: a small in-degree $K = 100$, and a rather large in-degree $K = 5000$. While the first case might be suitable for small functional networks, the latter in-degree represents a typical number for cortical networks. Further details

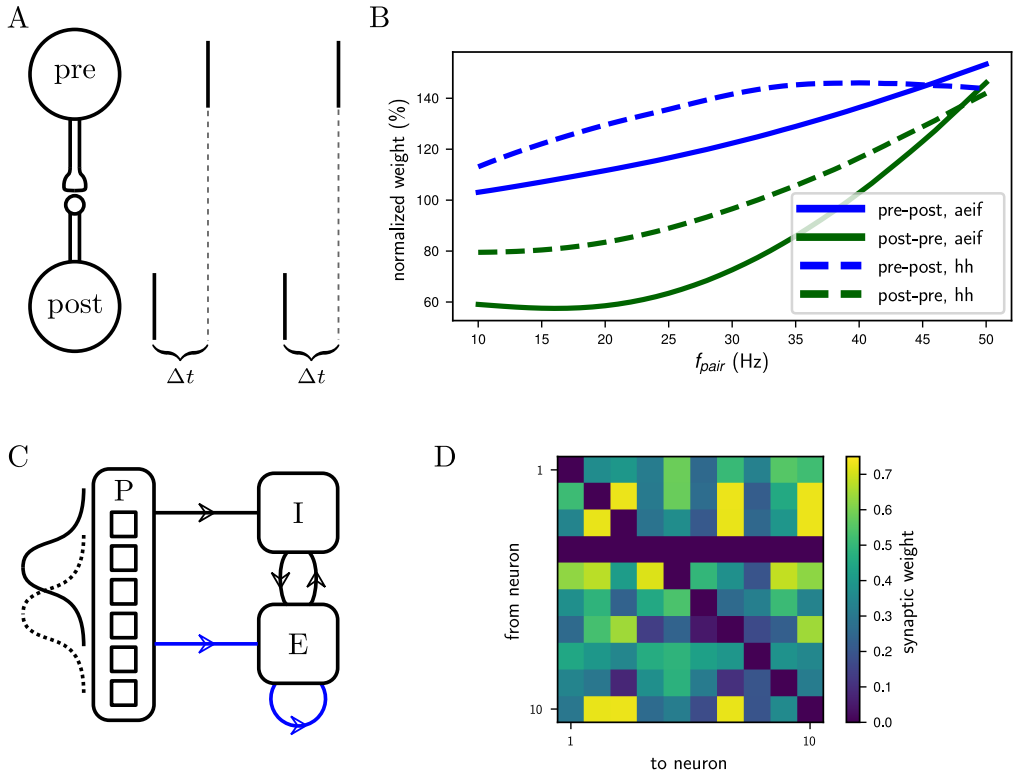

Figure 7. Reproduction of results with Clopath rule. A Setup of the spike pairing experiment. Two neurons ("pre" and "post") that are connected by a plastic synapse receive input so that they spike one after another with a delay Δt. The change of the synaptic weight is computed according to the Clopath rule as a function of the frequency f_{pair} with which the spike pairs are induced. **B** Result of the spike pairing experiment. The relative change of the synaptic weight after five spike pairs as a function of f_{pair} is shown for two different neuron models (aeif: solid lines, Hodgkin-Huxley: dashed lines). The blue lines represent a setup where the postsynaptic neuron fires after the presynaptic one (pre-post, $\Delta t = 10\,\text{ms}$) and the green lines represent the opposite case (post-pre, $\Delta t = -10\,\text{ms}$). This panel corresponds to figure 2b in **Clopath et al.** (2010). **C** Setup of the network that produces strong bidirectional couplings. The network consists of an inhibitory (I) and an excitatory (E) population which receive Poisson spike trains (P) as an external input. The firing rate of the latter is modulated with a Gaussian shape whose center is shifted every $100\,\text{ms}$. The external input connections to the excitatory population are plastic as well as the connections within the excitatory population (indicated by blue arrows). **D** Synaptic weights of the all-to-all connected excitatory neurons after the simulation of the network. Strong bidirectional couplings can be found, e.g. between neurons 2 and 3, 2 and 7, and 2 and 10. This panel corresponds to figure 5 in **Clopath et al.** (2010). A more detailed description of the two experiments can be found in Section 5.2.

on network and simulation parameters are given in Table 6. As a reference, we also simulate the same network with STDP synapses, which require much less computations as they rely solely on spike times. To achieve the same network state, that is the same spikes, for the different connectivity rules, we impose the weights to stay constant across time by setting learning rates to zero. This way all computations for weight changes are being performed, but just not applied. This has the additional advantage that reasonable asynchronous irregular network states are simple to find based on predictions for static synapses (**Brunel**, 2000).

The Clopath rule has originally been proposed for connections without delays (**Clopath et al.**, 2010). Therefore, we first evaluate its performance in this setting (delay equals simulation time step), which is, however, not the natural setting for a simulator like NEST that makes use of delays to speed up

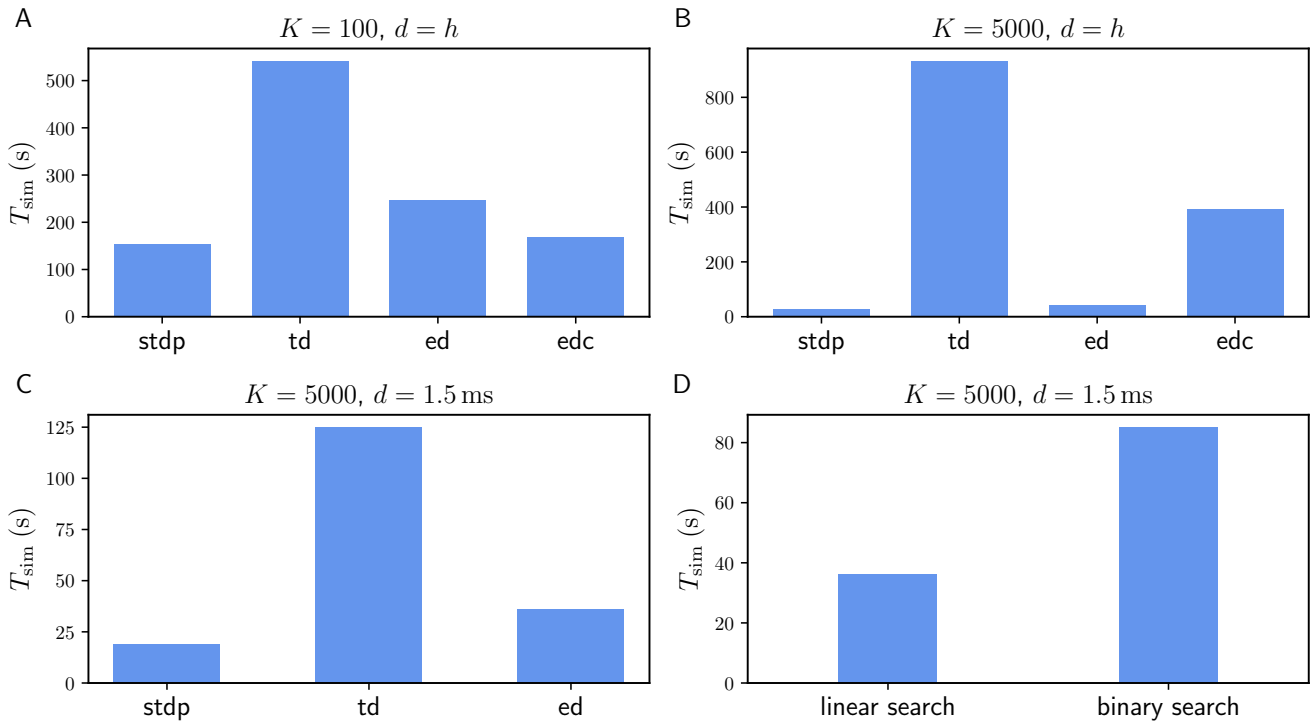

Figure 8. Comparison of state propagation times T_{sim} for excitatory-inhibitory networks with different implementations of the Clopath plasticity in NEST. The following implementations are shown: "stdp": standard implementation of STDP synapse, "td": time-driven implementation of Clopath synapse, "ed": event-driven scheme as included in NEST 2.18, "edc": event driven compression. **A** Network of size $N = 1.92 \cdot 10^6$ with small in-degree $K = 100$ and all synapses having a delay d equal to the resolution of the simulation h. **B** Network of size $N = 1.54 \cdot 10^5$ with large in-degree $K = 5000$ and $d = h$. **C** Same network as in panel B but $d = 1.5\,\text{ms}$ (for $d > h$ "edc" not compatible with NEST, see Section 2.3.3). In A, B, and C both "ed" and "edc" use linear search of the history and access counters, see 2.4.3. **D** Comparison between "ed"-implementations using linear search and binary search of the history. For all the simulations 768 threads were used over 32 compute nodes each running one MPI process. Further parameters as in Table 6.

communication between compute processes. The first observation is that, as expected, simulations with Clopath synapses are slower than those with ordinary STDP (Figure 8). Given the update of synapses in every simulation step, the time-driven scheme for Clopath synapses is much slower than the event-driven scheme (Figure 8A). The difference becomes larger the more synapses there are (Figure 8B). Introducing a delay leads to less function calls to synapses (once every `min_delay`) and therefore increases the speed of the time-driven scheme (Figure 8C). Its performance, however, stays much below the event-driven scheme. This comparison illustrates the benefit of event-driven updates for Clopath synapses.

How does compression of the history change the picture? As discussed in Section 2.3.3, compression has the advantage of not integrating the membrane potential history for each synapse separately. A downside of the event-based compression is that it requires storing one history entry for each last spike time of presynaptic neurons. For large in-degrees, this history is therefore longer than the history of $V^*_{i,\text{LTP}}$, which we implemented as non-continuous for the Clopath rule. Consequently, the event-based compression scheme only outperforms the ordinary event-driven scheme for small in-degrees (Figure 8A), but not for large in-degrees (Figure 8B). Given that the compression can only be implemented in NEST for connections with delay equal to the resolution of the simulation (see Section 2.4.4), the method of choice is therefore

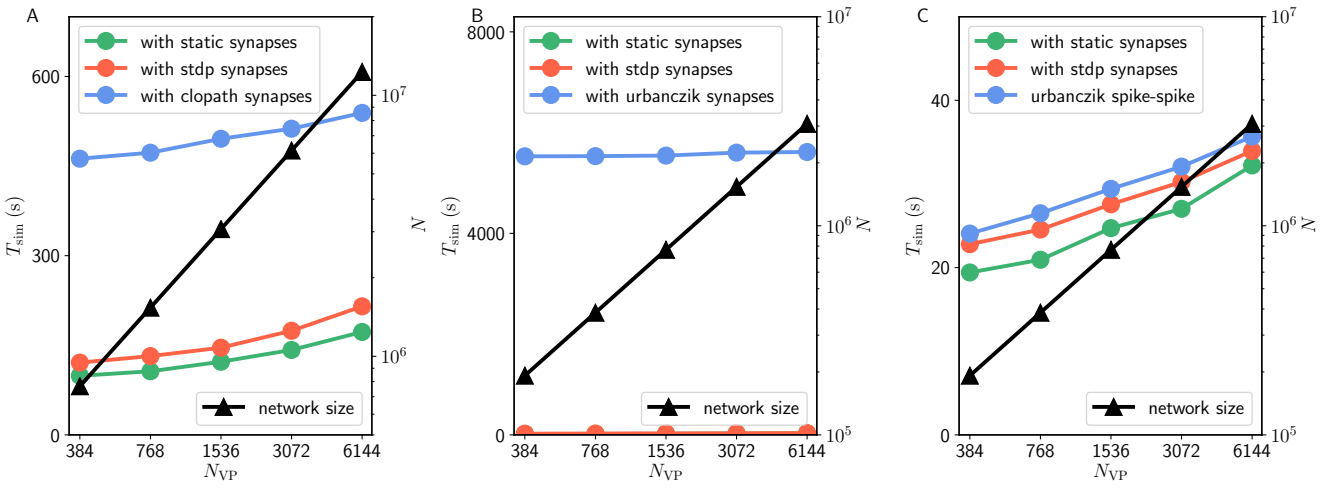

Figure 9. Scaling of state propagation times T_{sim} with network size for $2\,s$ of biological time. Weak scaling: computational resources (horizontal axes) are increased proportionally to network size N (black curve and triangles, right vertical axes). (**A**) Event-driven scheme for Clopath rule compared to static and STDP synapse. (**B**) Event-driven Urbanczik-Senn rule compared to static and STDP synapse. Due to the scale on the y-axis the green curve (static synapses) coincides with the red one (STDP synapses). (**C**) Spike-spike version of the Urbanczik-Senn rule compared to static and STDP synapse. Network and simulation parameters as in Table 6 with in-degree $K = 5000$. N_{VP} denotes the number of threads where every MPI process occupies one compute node and runs 24 threads.

the ordinary event-driven scheme (Section 2.3.2). Although a bit slower, its run-time is on the same order of magnitude as the ordinary STDP synapse, with similar weak-scaling behavior (Figure 9A). The additional computations with respect to STDP result in a constant overhead.

Another advantage of having short non-continuous histories is that searching the history at readout is fast. A simple linear iteration scheme is therefore even faster than a binary search (Figure 8D) because the latter search requires an additional list of presynaptic spike times (see Section 2.4.3) which is unnecessary overhead in this scenario. As a result the ordinary event-driven scheme with linear history iteration is the most general and efficient scheme and therefore integrated into NEST 2.18 (**Jordan et al.**, 2019).

3.2 Urbanczik-Senn plasticity

The Urbanczik-Senn rule (**Urbanczik and Senn**, 2014) applies to synapses that connect to dendrites of multicompartment model neurons. The main idea of this learning rule is to adjust the weights of dendritic synapses such that the dendrite can predict the firing rate of the soma. The dendrite expects the firing rate to be high when the dendrite's membrane potential is elevated due to many incoming spikes at the dendrite, and to be low if there are only a few incoming spikes. Thus, for this prediction to be true, synapses that transmit a spike towards the dendrite while the firing rate of the soma is low are depressed and those that provide input while the soma's firing rate is high are facilitated. Learning can be triggered by applying a teacher signal to the neuron via somatic synapses such that the actual somatic firing deviates from the dendritic prediction.

The plasticity rule is again of the general form (1), with a functional F on the right hand side that reads

$$F[s_j^*, V_i^*] = \eta\, \kappa * \left(V_i^*\, s_j^*\right) \tag{15}$$

$$\text{with } V_i^* = \left(s_i - \phi(V_i)\right)\, h\left(V_i\right), \tag{16}$$

$$s_j^* = \kappa_s * s_j.$$

with exponential filter kernels κ and κ_s and nonlinearities ϕ and h. Note that F depends on the postsynaptic spike train s_i via V_i^*. The latter can be interpreted as a prediction error, which never vanishes as spikes s_i (point process) are compared against a rate prediction $\phi(V_i)$ (continuous signal).

3.2.1 Implementation details of the Urbanczik-Senn rule

Following the original publication (**Urbanczik and Senn**, 2014), we here exemplify the Urbanczik-Senn rule with a two-compartment Poisson model neuron consisting of one somatic and one dendritic compartment (`pp_cond_exp_mc_urbanczik`). Extensions to multiple dendritic compartments are straight forward. In contrast to the implementation of a non-continuous history for the Clopath rule, a non-vanishing prediction error ($V_i^*(t) \neq 0$) here requires the storage of a continuous history. In order to solve (1), we need to integrate over $F[s_j^*, V_i^*]$ (cf. (2)). Writing down the convolution with κ explicitly, we obtain

$$\begin{aligned}\Delta W_{ij}(t,T) &= \int_t^T dt'\, F[s_j^*, V_i^*](t') \\ &= \int_t^T dt'\, \eta \int_0^{t'} dt'' \kappa\left(t' - t''\right) V_i^*\left(t''\right) s_j^*\left(t''\right).\end{aligned}$$

A straight forward implementation of this expression is very inefficient in terms of memory usage and computations because of the two nested integrals: The latter integral over t'' always starts at $t'' = 0$ which requires the synapse to evaluate the entire history of V_i^* and s_j^* whenever it performs a weight update. However, since the kernels κ and κ_s are exponentials, one can perform one of the integrations analytically (see appendix Section 5.4 for a derivation) to rewrite the weight change as

$$\Delta W_{ij}(t,T) = \eta\left[I_1\left(t,T\right) - I_2\left(t,T\right) + I_2\left(0,t\right)\left(1 - e^{-\frac{T-t}{\tau_\kappa}}\right)\right], \tag{17}$$

$$\text{with } I_1\left(a,b\right) = \int_a^b dt\, V_i^*\left(t\right) s_j^*\left(t\right),$$

$$I_2\left(a,b\right) = \int_a^b dt\, e^{-\frac{b-t}{\tau_\kappa}} V_i^*\left(t\right) s_j^*\left(t\right).$$

The first two integrals in (17) only extend from t to T; history entries for times smaller than t are not needed and can be deleted after the corresponding update. The dependence on the full history back until 0 arising from the convolution with κ is accumulated in the last term in (17), which can be computed by the synapse by storing one additional value $I_2\left(0,t\right)$. At the end of a weight update this value is overwritten by the new value $I_2\left(0,T\right) = e^{-\frac{T-t}{\tau_\kappa}} I_2\left(0,t\right) + I_2\left(t,T\right)$ which is then used in the next update.

(17) corresponds to the general formulation discussed in Figure 2 and can be dealt with as shown there. In particular, a history of $V_i^*\left(t\right)$ is stored and the integrals I_1 and I_2 are calculated within the synapse (time- and event-driven update) or the archiving node (event-driven update and compression).

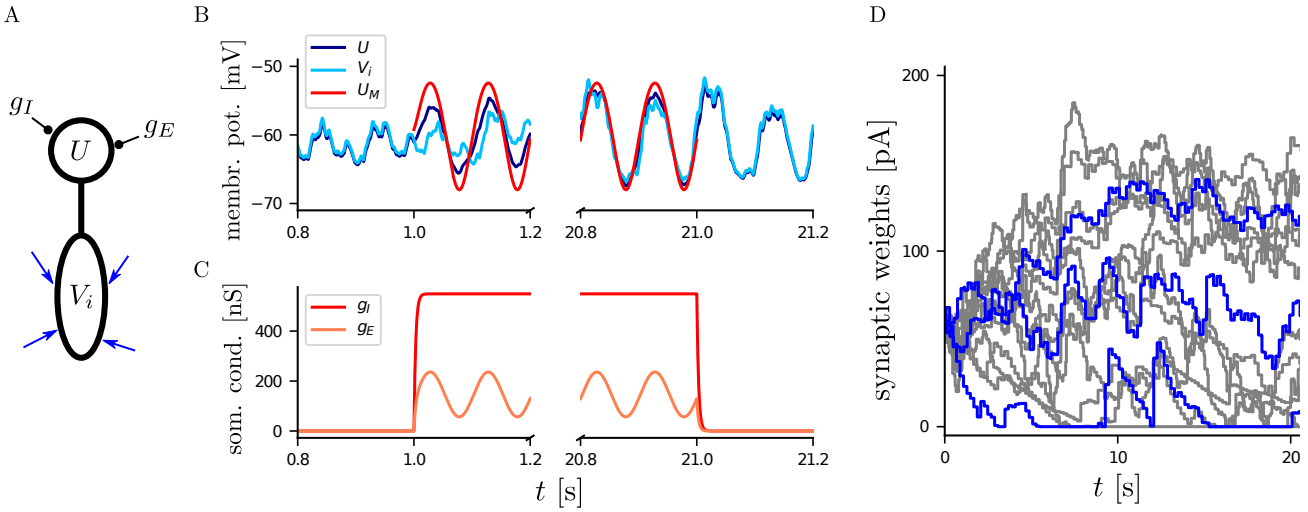

Figure 10. Reproduction of results with Urbanczik-Senn rule. A Setup of a simple learning task using the Urbanczik-Senn plasticity rule. The somatic conductances g_I and g_E of a two-compartment neuron are modulated such that they induce a teaching signal with sinusoidal shape. The dendrite receives a repeating spike pattern as an input via plastic synapses (blue arrows). **B** The synapses adapt their weights so that the somatic membrane potential U (dark blue) and the dendritic prediction V_i (light blue) follow the matching potential U_M (red) after learning. **C** Excitatory (g_E) and inhibitory (g_I) somatic conductances that produce the teaching signal. A and B corresponds to figure 1 in (**Urbanczik and Senn**, 2014). **D** Temporal evolution of the synaptic weights during learning. For the sake of better overview, only a subset of weights is shown (gray) with three randomly chosen time traces highlighted in blue. Synapses in NEST fulfill Dale's principle which means that a weight update cannot convert an excitatory into an inhibitory synapse and vice versa giving rise to the rectification at zero.

Since parameters of the functions ϕ and h in (16) are not only used for the plasticity rule, but also for the neuron dynamics, they are passed via a template class `pp_urbanczik_parameters` as an argument to the archiving node and the neuron model (see Section 2.4.1).

The basic use of the Urbanczik-Senn rule in NEST is exemplified in Appendix Section 5.5, which details the NEST setup and a reproduction of a simple learning experiment (Figure 10) from the original publication (**Urbanczik and Senn**, 2014).

3.2.2 Performance of the reference implementation

As for the Clopath rule, we employ a weak-scaling setup with the same excitatory-inhibitory networks of increasing size and fixed in-degree $K = 100$ or $K = 5000$, respectively (Table 6). We compare the results for the Urbanczik-Senn plasticity rule to networks with ordinary STDP synapses, again setting all learning rates to zero to achieve the same network state across different types of plasticity.

The Urbanczik-Senn rule, in its original version, does not account for delays in connections (**Urbanczik and Senn**, 2014). As for the Clopath rule, we therefore first evaluate its performance for connections with delays that equal the simulation time step. Naturally, the processing of the membrane potential information makes the Urbanczik-Senn plasticity less efficient to simulate than networks with ordinary STDP synapses (Figure 11). Note that the absolute numbers of simulation times are not directly comparable to simulations with Clopath plasticity (Figure 8) as network sizes are smaller here (Table 6). Networks with small and large in-degrees behave qualitatively similar: given the long continuous history that needs to be stored and read out, the event-driven scheme does not significantly outperform the time-driven scheme (Figure 11A,B). In the network with small in-degree, the time-driven scheme is even slightly faster (Figure 11A). This

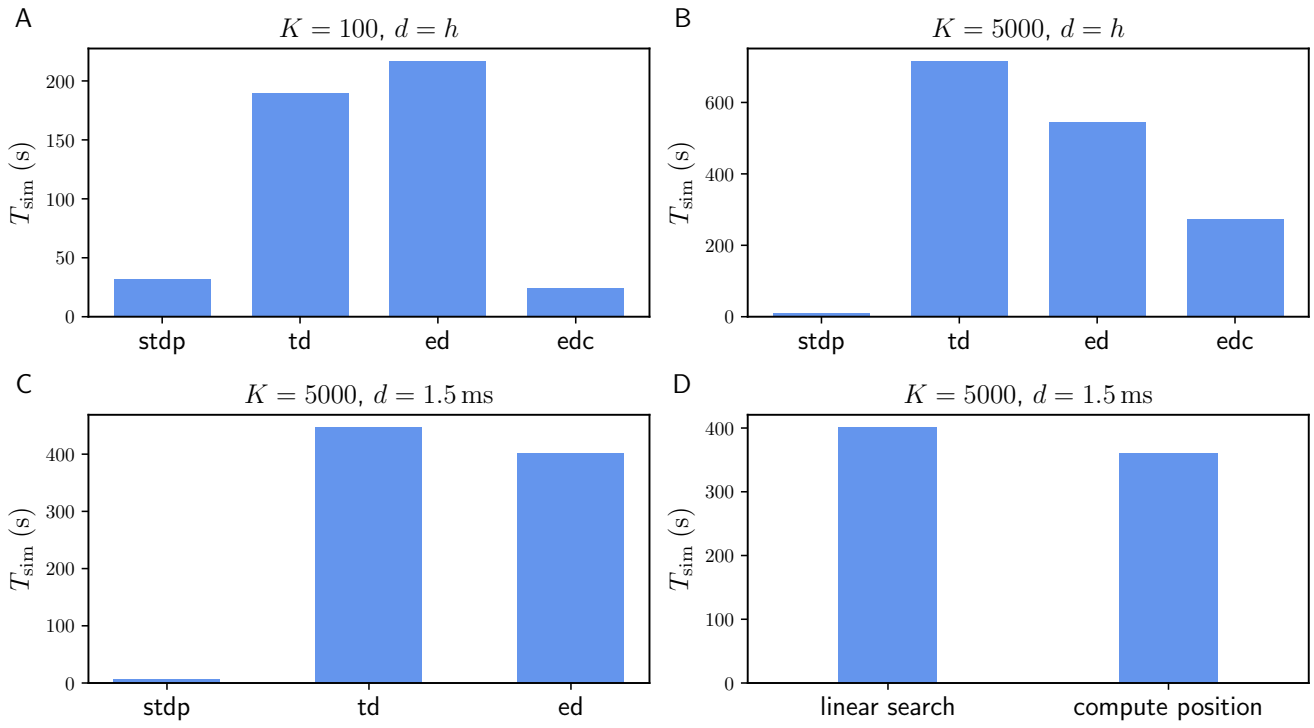

Figure 11. Comparison of state propagation times T_{sim} for excitatory-inhibitory networks with different implementations of the Urbanczik-Senn plasticity in NEST. The following implementations are shown: "stdp": standard implementation of STDP synapse in NEST, "td": time-driven implementation of Urbanczik-Senn synapse, "ed": event-driven scheme, "edc": event driven compression. **A** Network of size $N = 3.84 \cdot 10^5$ with small in-degree $K = 100$ and all synapses having a delay d equal to the resolution of the simulation h. **B** Network of size $N = 3.84 \cdot 10^4$ with large in-degree $K = 5000$ and $d = h$. **C** Same network as in panel B but $d = 1.5\,\text{ms}$ (for $d > h$ "edc" not compatible with NEST, see Section 2.3.3). In A, B, and C both "ed" and "edc" use linear search of the history and the access counters, see 2.4.3. **D** Comparison between "ed"-implementations using linear search and binary search of the history. For all the simulations 768 threads were used over 32 compute nodes each running one MPI-process. Details about the parameters used in these networks can be found in Table 6.

behavior reverses for large in-degrees as the number of synapse calls grows stronger than the length of the history (Figure 11B). However, given that the length of the history is so critical in this rule, the compression algorithm can in both cases achieve a significant increase in performance (Figure 11A,B). This performance increase is larger the smaller the in-degree, as the compressed history becomes shorter (Figure 11A). Due to NEST specificities (see Section 2.4.4), the compression algorithm cannot be used in settings with delays that are are larger than the simulation time step (Figure 11C): Here, as expected, the time-driven scheme becomes faster than in the $d = h$ case, but it is in general still comparable in performance to the event-driven scheme. The latter is therefore the method of choice for simulations with delayed connections; for zero-delay connections, the compression algorithm performs best. Consequently, both schemes are permanently integrated in NEST. Whether the history readout is done via linear iteration or via computing positions of history entries has no significant impact on the performance (Figure 11D). Therefore, the simple linear iteration is integrated in NEST 3.

3.3 Conclusions

The analyses of the Clopath and Urbanczik-Senn plasticity as prototypical examples for rules that rely on storage of discontinuous versus continuous histories show that the former are much faster to simulate, in particular for large networks that require distributed computing architectures. For discontinuous histories, the event-driven scheme is most generally applicable and efficient, which makes corresponding rules easy to integrate into modern simulators with event-based synapses. The performance gap between the different rules should be kept in mind in the design of new learning rules. Furthermore, it is worthwhile to test modifications of existing learning rules to decrease the amount of stored information.

For illustration, we here test a spike-based alternative to the original Urbanczik-Senn rule, where we replace the rate prediction $\phi\left(V_i\left(t\right)\right)$ in V^* of (16) by a noisy estimate, which we generate by a non-homogeneous Poisson generator with rate $\phi\left(V_i\left(t\right)\right)$, see Section 5.6. The prediction error then results in a comparison of somatic and dendritic spikes, s_i and s_i^{dend}, respectively; it is therefore purely based on point processes. In terms of storage and computations, the rule thereby becomes similar to ordinary STDP (cf. (5)). This becomes apparent in the weak-scaling experiment in Figure 9C, which shows that the modification of the learning rule results in a speedup of a factor 10 to 30 arriving essentially at the same run time as the ordinary STDP rule.

When changing learning rules to improve the efficiency of an implementation, the question is in how far the modified rule, in our example including the noisy estimate of the dendritic prediction, still fulfills the functionality that the original rule was designed for. Generally, without control of the error any simulation can be made arbitrarily fast. Therefore **Morrison et al.** (2007b) define efficiency as the wall-clock time required to achieve a given accuracy. We test in the appendix (Fig. 1 Figure 12) whether the dynamics is still robust enough to achieve proper learning and function in the reproduced task of Figure 10. The learning works as well as in the original Urbanczik-Senn rule. However, given the simplicity of the chosen task , this result may not generalize to other more natural tasks. We leave a more detailed investigation of this issue to future studies. The basic exploration here, however, illustrates how taking into account the efficiency of implementations can guide future development of learning rules to make them practically usable for large-scale simulations of brain networks.

4 DISCUSSION

This work presents efficient algorithms to implement voltage-based plasticity in modern neural network simulators that rely on event-based updates of synapses (for a review, see **Brette et al.**, 2007). This update scheme restricts function calls of synapse code to time points of spike events and thereby improves performance in simulations of biologically plausible networks, where spike events at individual synapses are rare and the total number of synapses is large compared to the number of neurons. In voltage-based plasticity rules, synapses, however, rely on continuous information of state variables of postsynaptic cells to update their strength, which naturally suggests their time-driven update. Instead, we here propose an efficient archiving of voltage traces to enable event-based synapse updates and detail two schemes for storage, read out and post-processing of time-continuous or discontinuous information. We show their superior performance with respect to time-driven update both theoretically and with a reference implementation in the neural network simulation code NEST for the rules proposed in **Clopath et al.** (2010) and **Urbanczik and Senn** (2014).

Event-driven update schemes for voltage-based plasticity come at the expense of storing possibly long histories of a priori continuous state variables. Such histories not only require space in memory but they

also affect the runtime of simulations, which we focus on here. The time spent for searching and post-processing the history to calculate weight updates increases with increasing length, and these operations have to be done for each synapse. Therefore, in addition to an ordinary event-driven scheme, we devised a compression scheme that becomes superior for long histories as occurring in the Urbanczik-Senn rule. In particular for networks with small in-degrees or synchronous spiking, the compression scheme results in a shorter history. It further reduces the total amount of computations for weight changes by partially re-using results from other synapses thereby avoiding multiple processing of the history. For short histories as occurring in the Clopath rule, the compression results in unnecessary overhead and an increase in history size as one entry per last presynaptic spike time needs to be stored instead of a discontinuous membrane potential around sparse postsynaptic spike events. We here, for simplicity, contrasted time- and event-driven update schemes. However, further work could also investigate hybrid schemes, where synapses are not only updated at spike events, but also on a predefined and coarse time grid to avoid long histories and corresponding extensive management. A similar mechanism is used in **Kunkel et al.** (2011) to implement a normalization of synaptic weights. The corresponding technical details can be found in **Kunkel** (2015, ch. 5.2).

The storage and management of the history as well as complex weight change computations naturally reduce the performance of simulations with voltage-based plasticity in comparison to static or STDP synapses. The latter only require information on spike times which is much less data compared to continuous signals. Nevertheless, given that the Clopath rule is based on thresholded membrane potentials and consequently short, discontinuous histories, the performance and scaling of the event-driven algorithms is only slightly worse than for ordinary STDP. Time-driven implementations cannot employ this model feature and update weights also in time steps where no adjustment would be required, leading to significantly slower simulations. The performance gain of using event-driven schemes is less pronounced for the Urbanczik-Senn rule as, by design, histories are typically long. In this case, the compression scheme naturally yields better results in terms of runtime. Our own sampling-based modification of the Urbanczik-Senn rule only requires storage of the membrane potentials at spike events, giving rise to the same performance as STDP. Generally, an algorithm is faster if it requires less computations. However, opportunities for vectorization and cache efficient processing, outside of the scope of the present manuscript, may change the picture.

We here chose the Clopath and the Urbanczik-Senn rule as two prototypical models of voltage-based plasticity. While both rules describe a voltage dependence of weight updates, their original motivation as well as their specific form are different: The Clopath rule refines standard STDP models to capture biologically observed phenomena such as frequency dependence of weight changes (**Sjöström et al.**, 2001). For this it is sufficient to take into account membrane potential traces in the vicinity of spike events, leading to storage of time-discontinuous histories in our implementation. In contrast, the Urbanczik-Senn rule is functionally inspired by segregating dendritic and somatic compartments of cells and using the difference between somatic output and dendritic prediction as a teacher signal for dendritic synapses. The teacher signal is by construction never vanishing, imposing the need to store a time-continuous history. The original publications of both rules had a great and long-lasting impact on the field. The Clopath rule has been used in a variety of studies (**Clopath and Gerstner**, 2010; **Ko et al.**, 2013; **Litwin-Kumar and Doiron**, 2014; **Sadeh et al.**, 2015; **Bono and Clopath**, 2017; **Maes et al.**, 2020), partly in modified versions which are, however, still compatible with the here presented simulation algorithms. The same holds for the Urbanczik-Senn rule (**Brea et al.**, 2016; **Sacramento et al.**, 2018).

The current implementation in NEST supports an adaptive exponential integrate-and-fire and a Hodgkin-Huxley neuron model for the Clopath rule. The former is used in the original publication (**Clopath**

et al., 2010) and the latter appears on ModelDB (**Hines et al.**, 2004) in code for the Clopath rule for the NEURON simulator (**Hines and Carnevale**, 2001). For the Urbanczik-Senn rule, NEST currently supports the two-compartment Poisson model neuron of the original publication (**Urbanczik and Senn**, 2014). A three-compartment version as used in **Sacramento et al.** (2018) or other models are straight forward to integrate into the current simulation framework. However, with voltage-based plasticity rules, borders between neurons and synapses become blurred as these rules often depend on specificities of the employed neuron models rather than only spike times as for standard STDP. Consequently, archiving nodes might need to have specific functionalities, which, in light of the zoo of existing neuron models, could easily lead to a combinatorial explosion of code. These problems can in future be overcome with automatic code generation using NESTML that only creates and compiles code that is needed for the specified model simulations (**Plotnikov et al.**, 2016).

While the here presented implementation refers to the neural network simulator NEST (**Gewaltig and Diesmann**, 2007), the proposed algorithms and simulation infrastructure are compatible with any network simulator with event-driven update of synapses, such as, for example, NEURON (**Lytton et al.**, 2016, cf. ch. 2.4) and Brian2 (**Stimberg et al.**, 2014). Furthermore, applicability is not restricted to the Clopath and Urbanczik-Senn rule, but the framework can be adapted to any other learning rule that relies on state variables of postsynaptic neurons. State variables hereby not only encompass membrane potentials such as, for example, in the LCP rule by **Mayr and Partzsch** (2010), the Convallis rule by **Yger and Harris** (2013), the voltage-triple rule by **Brea et al.** (2013), the MPDP rule by **Albers et al.** (2016), the neuromorphic learning rules by **Sheik et al.** (2016) and **Diederich et al.** (2018), or the branch-specific rule by **Legenstein and Maass** (2011), but also, for example, firing rates of stochastic neuron models or rate models (**Brea et al.**, 2016; **Sacramento et al.**, 2018), or other learning signals (**Bellec et al.**, 2019). The same machinery could be also used to store external teacher signals that are provided to model neurons by stimulation devices. Since synapses are located at the compute process of the postsynaptic neuron, readout of state variables from presynaptic neurons comes with large costs in simulations on distributed computing architectures and is therefore not considered here. Due to specificities of the present NEST code in spike delivery, the event-driven compression proposed here is only applicable in NEST for delays that equal the simulation time step. Such a restriction can be readily overcome in a simulation algorithm that performs a chronological update of synapses.

In general, one has to distinguish two types of efficiency in the context of simulating plastic networks: Firstly, the biological time it takes the network to learn a task by adapting the weights of connections. Secondly, the wall-clock time it takes to simulate this learning process. Both times crucially depend on the employed plasticity rule. In this study, we focused on the wall-clock time and argue that this can be optimized by designing learning rules that require storing only minimal information on postsynaptic state variables. Ideally, the plasticity rule contains unfiltered presynaptic or postsynaptic spike trains to reach the same performance as in ordinary STDP simulations. If rules, however, need to capture the pre- and post-spike dynamics of postsynaptic neurons, it is beneficial to make use of thresholded state variables as in the example of the Clopath rule as this yields short, time-discontinuous histories. Reducing the amount of information available for synapses to adjust their weights can in general slow down the learning. We presented a modification of the Urbanczik-Senn rule where the dendritic prediction of the somatic firing contains an additional sampling step with Poisson spike generation. This modification significantly reduces the simulation time. For the here presented simple task, learning speed is largely unaffected, but generally a performance decrease is to be expected when error signals become more noisy. Therefore, there is a trade-off between learning speed and simulation speed, which should be considered in the design process of new learning rules.

For the plasticity rules by **Clopath et al.** (2010) and **Urbanczik and Senn** (2014), we present a highly scalable reference implementation in NEST. The parallelism of the NEST implementation enables simulations of plastic networks of realistic size on biologically plausible time scales for learning. The field of computational neuroscience recently entered a new era with development of large-scale network models (**Markram et al.**, 2015; **Schmidt et al.**, 2018; **Billeh et al.**, 2020). Emulating the dynamics of cortical networks, such models are so far restricted to static connections. We here provide simulation algorithms for plasticity mechanisms that are required for augmenting such complex models with functionality. It is our hope that incorporating both biologically and functionally inspired plasticity models in a single simulation engine fosters the exchange of ideas between communities towards the common goal of understanding system-level learning in the brain.

CONFLICT OF INTEREST STATEMENT

The authors declare that the research was conducted in the absence of any commercial or financial relationships that could be construed as a potential conflict of interest.

ACKNOWLEDGMENTS

We thank Claudia Clopath and Wulfram Gerstner for explaining details of their reference implementation and the underlying biological motivation. Moreover, we thank Hedyeh Rezaei and Ad Aertsen for suggesting to implement the Clopath rule in NEST and Charl Linssen, Alexander Seeholzer, Renato Duarte for carefully reviewing our implementation. Finally we thank Walter Senn, Mihai A. Petrovici, Laura Kriener and Jakob Jordan for fruitful discussions on the Urbanczik-Senn rule and our proposed spike based version. We further gratefully acknowledge the computing time on the supercomputer JURECA (**Jülich Supercomputing Centre**, 2015) at Forschungszentrum Jülich granted by firstly the JARA-HPC Vergabegremium (provided on the JARA-HPC partition, jinb33) and secondly by the Gauss Centre for Supercomputing (GCS) (provided by the John von Neumann Institute for Computing (NIC) on the GCS share, hwu12). This project has received funding from the Helmholtz Association Initiative and Networking Fund under project number SO-092 (Advanced Computing Architectures, ACA) and the European Union's Horizon 2020 research and innovation programme under grant agreements No 785907 (HBP SGA2) and No 945539 (HBP SGA3). Partly supported by the Helmholtz young investigator group VH-NG-1028. All network simulations carried out with NEST (http://www.nest-simulator.org). This work was supported by the Jülich-Aachen Research Alliance Center for Simulation and Data Science (JARA-CSD) School for Simulation and Data Science (SSD).

5 APPENDIX

5.1 Voltage clamping of the adaptive exponential integrate-and-fire model

For the Clopath rule the change of the synaptic weight strongly depends on the excursion of the membrane potential V_m around a spike of the postsynaptic neuron which causes $\bar{u}_\pm$ to cross the respective thresholds $\theta_\pm$ so that (13) and (14) yield nonvanishing results. Within the original neuron model (**Brette and Gerstner**, 2005) u is reset immediately after it reached the spiking threshold so that the shape of the action potential is not described accurately. In our NEST implementation of `aeif_psc_delta_clopath` we adapted the approach of the reference implementation on ModelDB (**Hines et al.**, 2004) and introduced a clamping of u to a fixed value V_{clamp} for a period of t_{clamp} before it is reset. The reference implementation is restricted to a simulation resolution of exactly $1\,\text{ms}$ and sets u to two different values for the two subsequent simulation

steps after a spike. To be independent of the resolution of the simulation, the implementation in NEST uses a constant V_{clamp}. In the simulations we set t_{clamp} to $2\,\text{ms}$ and V_{clamp} to $33\,\text{mV}$. These values are chosen to match the behavior of the reference implementation.

5.2 Implementation of experiments using Clopath rule

5.2.1 Spike pairing experiment

The setup of the spike pairing experiment from **Clopath et al.** (2010) presented in Figure 7A,B consists of two neurons connected via a plastic synapse. The pre- and postsynaptic neuron are forced to spike with a time delay of Δt by stimulation with `spike_generators` at times $t_{\text{pre}}^{(i)} = t^{(i)}$ and $t_{\text{post}}^{(i)} = t^{(i)} + \Delta t$, respectively. A positive time shift $\Delta t > 0$ refers to the presynaptic neuron spike before the postsynaptic one (pre-post pairing, solid lines in Figure 7) and vice versa. Spike pairs $\left(t_{\text{pre}}^{(i)}, t_{\text{post}}^{(i)}\right)$ are induced with frequency $f_{\text{pair}} = \frac{1}{t^{(i+1)} - t^{(i)}}$ and the weight change of the synapse is measured after a set of five pairs. In our simulation using NEST the presynaptic neuron is modeled as a `parrot_neuron` and the postsynaptic neuron is either of type `aeif_psc_delta_clopath` or `hh_psc_alpha_clopath`. In NEST `parrot_neurons` are model neurons that emit a spike whenever they receive one. In this setup they are required because devices like `spike_generators` support only static synapses in NEST so that we cannot connect the postsynaptic neuron directly to the `spike_generator` via a plastic synapse. The initial weight of the `clopath_synapse` connecting the two neurons is given by w_{init}. In this experiment we use the Clopath rule with fixed amplitude A_{LTD}. A list with all the parameters can be found in Table 2.

5.2.2 Emergence of strong bidirectional couplings

In this experiment after **Clopath et al.** (2010), a small network of N_I inhibitory and N_E excitatory neurons subject to an external input develops strong bidirectional couplings between neurons of the excitatory population. The input is given by N_{p} Poisson spike trains with rates

$$f_{\text{p}}^{(j)} = A_{\text{p}} e^{-\frac{(j-\mu_{\text{p}})^2}{2\sigma_{\text{p}}^2}} + c_{\text{p}}, \tag{18}$$

where $j = 1, \ldots, N_{\text{p}}$. The center μ_{p} of the Gaussian is drawn randomly from a set s_{p} of possible values and a new value is drawn after each time interval t_μ. The total number of intervals is N_μ. In our simulation with NEST we used `aeif_psc_delta` model neurons with the same parameters (cf. Table 4) for both the inhibitory and the excitatory population. The simulation is divided into N_μ intervals between which the rates of the N_{p} `poisson_generators` are set according to (18). The `poisson_generators` are connected in a one-to-one manner to N_{p} `parrot_neurons` which in turn are connected to the network. The details of the latter connectivity can be found in Table 3. In NEST a `poisson_generator` that is connected to several target model neurons generates an independent Poisson spike train for each of these neurons. Thus, the intermediate step via `parrot_neurons` is required to provide neurons in the network with common Poisson inputs. Moreover, a direct connection from a device like a `poisson_generator` to a model neuron via a plastic synapse is not possible in NEST. In this experiment, the Clopath rule with homeostasis (time dependent prefactor for LTD, cf. Section 5.3) is used. Figure 7 C shows the weights of the synapses among the excitatory population after the simulation.

5.3 Implementation of homeostasis $A_{\mathrm{LTD}}(\bar{\bar{u}})$

For the network simulations presented in **Clopath et al.** (2010), the authors use a sightly modified version of the Clopath rule defined in (13): The constant factor A_{LTD} is replaced by a voltage dependent term

$$A_{\mathrm{LTD}}(\bar{\bar{u}}) = A_{\mathrm{LTD}} \left(\frac{\bar{\bar{u}}}{u_{\mathrm{ref}}} \right)^2$$

to take into account homeostatic processes. The quantity $\bar{\bar{u}}$ is a temporal average of the quantity $\bar{u}_-(t)$ over a time window of $T = 1\ s$ and u_{ref} is a reference value. An exact temporal average requires to store the time trace of $\bar{u}_-(t)$ for the entire interval T. This would cancel the advantage of the implementation discussed in Section 3.1 where storage of time traces is needed only in the vicinity of spikes. Therefore, deviating from the original work by **Clopath et al.** (2010), we implement an additional low-pass filtering $\bar{\bar{u}}(t) = (\kappa_{\mathrm{low}} * \bar{u}_-)(t)$ with an exponential kernel $\kappa_{\mathrm{low}}(t) = H(t) \exp(-t/\bar{\bar{\tau}})$ instead. Like $\bar{u}_\pm$, $\bar{\bar{u}}$ is passed as an additional state variable to the solver.

5.4 Analytical integration in Urbanczik-Senn rule

To derive 17 it is convenient to first investigate $\Delta W_{ij}(0,t)$ and $\Delta W_{ij}(0,T)$ and then compute $\Delta W_{ij}(t,T) = \Delta W_{ij}(0,T) - \Delta W_{ij}(0,t)$. Assuming that the simulation starts at $t = 0$, the weight change from the start to time t is given by

$$\begin{aligned}
\Delta W_{ij}(0,t) &= \eta \int_0^t dt' \int_0^{t'} dt'' \kappa(t'-t'') V_i^*(t'') s_j^*(t'') \\
&= \eta \int_0^t dt'' \int_{t''}^t dt' \kappa(t'-t'') V_i^*(t'') s_j^*(t'') \\
&= \eta \int_0^t dt'' \left[\tilde{\kappa}(t-t'') - \tilde{\kappa}(0) \right] V_i^*(t'') s_j^*(t'') \\
&= \eta \left[-I_2(0,t) + I_1(0,t) \right]
\end{aligned}$$

where we exchanged the order of integration from the first to the second line. In the third line we introduced $\tilde{\kappa}(t)$ defined by $\kappa(t) = \frac{\partial}{\partial t}\tilde{\kappa}(t)$ and in the fourth line we defined the two integrals

$$I_1(t_1,t_2) = -\int_{t_1}^{t_2} dt' \tilde{\kappa}(0) V_i^*(t') s_j^*(t'), \qquad I_2(t_1,t_2) = -\int_{t_1}^{t_2} dt' \tilde{\kappa}(t-t') V_i^*(t') s_j^*(t').$$

In case of the Urbanczik-Senn rule

$$\tilde{\kappa}(t) = -e^{-\frac{t}{\tau_\kappa}}$$

which implies the identities

$$I_1(t_1, t_2+\Delta t) = I_1(t_1,t_2) + I_1(t_2, t_2+\Delta t), \quad I_2(t_1,t_2+\Delta t) = e^{-\frac{t_2-t_1}{\tau_\kappa}} I_2(t_1,t_2) + I_2(t_2,t_2+\Delta t),$$

which we use to write the weight change from t to T as

$$\begin{aligned}\Delta W_{ij}(t,T) &= \Delta W_{ij}(0,T) - \Delta W_{ij}(0,t) \\ &= \eta\left[-I_2\left(0,T\right) + I_1\left(0,T\right) + I_2\left(0,t\right) - I_1\left(0,t\right)\right] \\ &= \eta\left[I_1\left(t,T\right) - I_2\left(t,T\right) + I_2\left(0,t\right)\left(1 - e^{-\frac{T-t}{\tau_\kappa}}\right)\right].\end{aligned}$$

This is the the result 17.

5.5 Implementation of experiment using Urbanczik-Senn rule

In the simulation experiment shown in Figure 10 the dendrite of a conductance-based two-compartment model neuron receives a spike pattern of duration T as an input via plastic synapses. The pattern consists of N_p independent Poisson spike trains with a firing rate f_p. For learning, the pattern is repeated N_rep times. Dendritic synapses adapt their weights so that after learning the somatic membrane potential U and the dendritic prediction V_w^* follow a matching potential U_M. The latter is created by somatic input via two `spike_generators` that are connected via a static excitatory or inhibitory connection, respectively. Both spike generators send spikes in every simulation step. Inhibitory input spikes have a constant weight to generate a constant somatic inhibitory conductance g_I. Excitatory spikes have a modulated weight to generate a periodic excitatory conductance g_E. The input to the dendritic compartment is provided by N_p `spike_generators` each of which is connected to one `parrot_neuron` which in turn is connected to the dendrite via a plastic `urbanczik_synapse`. The intermediate parrot_neurons are required since in NEST the spike_generators can have only static synapses as outgoing connections. The spike times of the `spike_generators` are set to repeatedly generate the spike pattern created before the start of the actual simulation. The neuron's state variables are read out by a `multimeter` and the synaptic weights by a `weight_recorder`.

5.6 Experiment with modified version of the Urbanczik-Senn rule

The weight change of the Urbanczik-Senn rule as presented in Section 3.2 in line with the original publication is driven by the prediction error

$$V_i^* = \left(s_i - \phi(V_i)\right)\, h\left(V_i\right),$$

where s_i is the somatic spike train and V_i the dendritic prediction of the somatic membrane potential U_i. Instead of integrating over the difference between the spike train and the rate $\phi\left(V_i\right)$ (spike-rate), one can derive two variants

$$\begin{aligned}V_i^* &= \left(s_i - s_i^\mathrm{dend}\right)\, h\left(V_i\right) \quad (\mathrm{spike} - \mathrm{spike}) \quad \text{and} \\ V_i^* &= \left(\phi\left(U_i\right) - \phi\left(V_i\right)\right)\, h\left(V_i\right) \quad (\mathrm{rate} - \mathrm{rate}).\end{aligned}$$

In the first one (spike-spike) we replaced the dendritic rate prediction by a noisy realization s_i^dend using an inhomogeneous Poisson process with rate $\phi\left(V_i\right)$. In the second one (rate-rate) the somatic spike train is replaced by the rate of the underlying Poisson process which is computed by applying the rate function ϕ to the somatic potential U_i. The learning of a matching potential U_M as described in Section 5.5 also works in these two cases. Figure 12 shows the learning curve for all three variants of the Urbanczik-Senn rule. The loss is defined as the average mismatch between U_i and U_M averaged over one period T_p of the

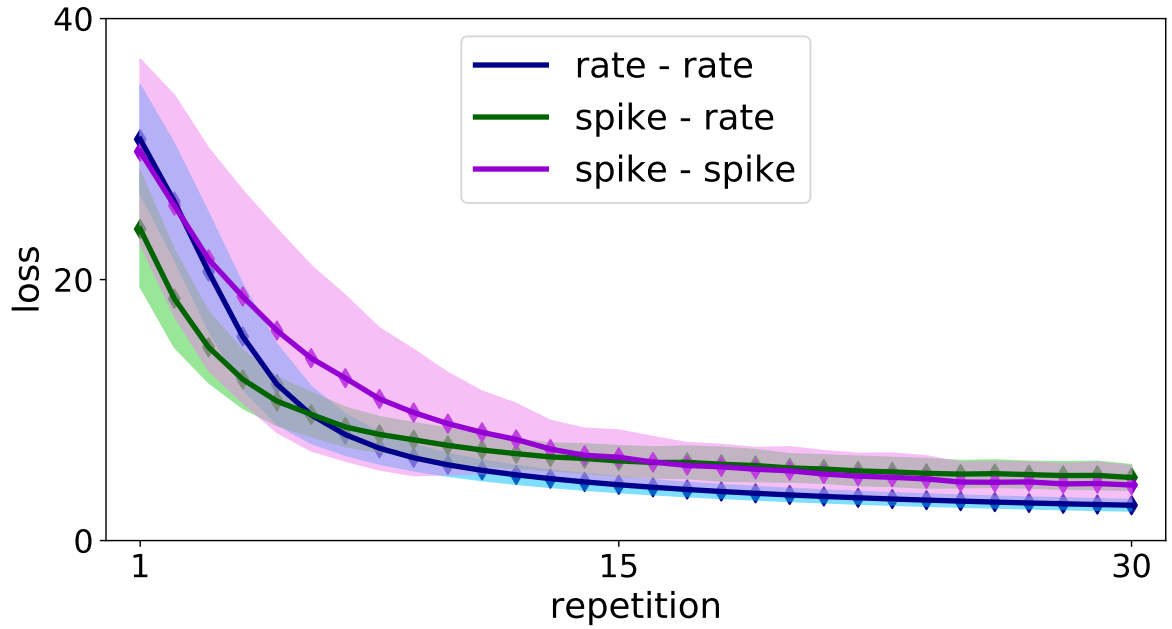

Figure 12. Comparison of learning curves in the experiment described in Section 5.5 for different variants of the Urbanczik-Senn plasticity rule. The loss is averaged over 128 trials of different input patterns. Solid curves denote the mean value and the shaded area the corresponding standard deviation of the loss.

input pattern

$$\frac{1}{T_p}\int dt\,(U\,(t)-U_M\,(t))^2\,.$$

The decrease of the loss as a function of the pattern repetitions has a similar shape for all three variants with a significantly higher variance in case of the spike-spike version.

REFERENCES

Albers, C., Westkott, M., and Pawelzik, K. (2016), Learning of precise spike times with homeostatic membrane potential dependent synaptic plasticity, *PLOS ONE*, 11, 2, 1–28, doi:10.1371/journal.pone.0148948

Bellec, G., Scherr, F., Subramoney, A., Hajek, E., Salaj, D., Legenstein, R., et al. (2019), A solution to the learning dilemma for recurrent networks of spiking neurons, *bioRxiv*, 738385

Bi, G. and Poo, M. (1998), Synaptic modifications in cultured hippocampal neurons: Dependence on spike timing, synaptic strength, and postsynaptic cell type, *J. Neurosci.*, 18, 10464–10472

Billeh, Y. N., Cai, B., Gratiy, S. L., Dai, K., Iyer, R., Gouwens, N. W., et al. (2020), Systematic integration of structural and functional data into multi-scale models of mouse primary visual cortex, *Neuron*

Bono, J. and Clopath, C. (2017), Modeling somatic and dendritic spike mediated plasticity at the single neuron and network level, *Nat. Commun.*, 8, 1, 1–17

Brea, J., Gaal, A. T., Urbanczik, R., and Senn, W. (2016), Prospective coding by spiking neurons, *PLOS Comput. Biol.*, 12, 6, 1–25, doi:10.1371/journal.pcbi.1005003

Brea, J., Senn, W., and Pfister, J.-P. (2013), Matching recall and storage in sequence learning with spiking neural networks, *J. Neurosci.*, 33, 23, 9565–9575

Brette, R. and Gerstner, W. (2005), Adaptive exponential integrate-and-fire model as an effective description of neuronal activity, *J. Neurophysiol.*, 94, 5, 3637–3642

Brette, R., Rudolph, M., Carnevale, T., Hines, M., Beeman, D., Bower, J. M., et al. (2007), Simulation of networks of spiking neurons: A review of tools and strategies, *J. Comput. Neurosci.*, 23, 3, 349–398, doi:10.1007/s10827-007-0038-6

Brunel, N. (2000), Dynamics of sparsely connected networks of excitatory and inhibitory spiking neurons, *Journal of Computational Neuroscience*, 8, 3, 183–208, doi:10.1023/a:1008925309027

Clopath, C., Büsing, L., Vasilaki, E., and Gerstner, W. (2010), Connectivity reflects coding: a model of voltage-based STDP with homeostasis, *Nat. Neurosci.*, 13, 344–352

Clopath, C. and Gerstner, W. (2010), Voltage and spike timing interact in stdp–a unified model, *Frontiers in synaptic neuroscience*, 2, 25

Davison, A., Brüderle, D., Eppler, J., Kremkow, J., Muller, E., Pecevski, D., et al. (2008), PyNN: a common interface for neuronal network simulators, *Front. Neuroinformatics*, 2, 11, doi:10.3389/neuro.11.011.2008

Diederich, N., Bartsch, T., Kohlstedt, H., and Ziegler, M. (2018), A memristive plasticity model of voltage-based stdp suitable for recurrent bidirectional neural networks in the hippocampus, *Scientific reports*, 8, 1, 1–12

Djurfeldt, M., Davison, A. P., and Eppler, J. M. (2014), Efficient generation of connectivity in neuronal networks from simulator-independent descriptions, *Front. Neuroinformatics*, 8, 43, doi:10.3389/fninf.2014.00043

Djurfeldt, M., Hjorth, J., Eppler, J. M., Dudani, N., Helias, M., Potjans, T. C., et al. (2010), Run-time interoperability between neuronal network simulators based on the MUSIC framework, *Neuroinformatics*, 8, 43–60

Eppler, J. M., Helias, M., Muller, E., Diesmann, M., and Gewaltig, M. (2009), PyNEST: a convenient interface to the NEST simulator, *Front. Neuroinformatics*, 2, 12, doi:10.3389/neuro.11.012.2008

Gerstner, W., Kempter, R., van Hemmen, J. L., and Wagner, H. (1996), A neuronal learning rule for sub-millisecond temporal coding, *Nature*, 383, 76–78

Gerstner, W., Kistler, W. M., Naud, R., and Paninski, L. (2014), Neuronal Dynamics. From single Neurons to Networks and Models of Cognition (Cambridge University Press, Cambridge)

Gewaltig, M.-O. and Diesmann, M. (2007), NEST (NEural Simulation Tool), *Scholarpedia*, 2, 4, 1430, doi:10.4249/scholarpedia.1430

Hannun, A., Case, C., Casper, J., Catanzaro, B., Diamos, G., Elsen, E., et al. (2014), Deep speech: Scaling up end-to-end speech recognition, *arXiv preprint arXiv:1412.5567*

Hebb, D. O. (1949), The organization of behavior: A neuropsychological theory (John Wiley & Sons, New York)

Hines, M. L. and Carnevale, N. T. (2001), NEURON: a tool for neuroscientists, *Neuroscientist*, 7, 2, 123–135, doi:10.1177/107385840100700207

Hines, M. L., Morse, T., Migliore, M., Carnevale, N. T., and Shepherd, G. M. (2004), ModelDB: A database to support computational neuroscience, *J. Comput. Neurosci.*, 17, 1, 7–11, doi:10.1023/B:JCNS.0000023869.22017.2e

Hinton, G. E., Osindero, S., and Teh, Y.-W. (2006), A fast learning algorithm for deep belief nets, *Neural computation*, 18, 7, 1527–1554

Jordan, J., Ippen, T., Helias, M., Kitayama, I., Sato, M., Igarashi, J., et al. (2018), Extremely scalable spiking neuronal network simulation code: From laptops to exascale computers, *Front. Neuroinformatics*, 12, 2, doi:10.3389/fninf.2018.00002

Jordan, J., Mørk, H., Vennemo, S. B., Terhorst, D., Peyser, A., Ippen, T., et al. (2019), Nest 2.18.0, doi:10.5281/zenodo.2605422

Jülich Supercomputing Centre (2015), JUQUEEN: IBM Blue Gene/Q® supercomputer system at the Jülich Supercomputing Centre

Ko, H., Cossell, L., Baragli, C., Antolik, J., Clopath, C., Hofer, S. B., et al. (2013), The emergence of functional microcircuits in visual cortex, *Nature*, 496, 7443, 96–100

Krizhevsky, A., Sutskever, I., and Hinton, G. E. (2012), Imagenet classification with deep convolutional neural networks, in Advances in neural information processing systems, 1097–1105

Kunkel, S. (2015), Simulation technology for plastic neuronal networks on high-performance computers, 10.6094/UNIFR/10419, 1–188, doi:10.6094/UNIFR/10419

Kunkel, S., Diesmann, M., and Morrison, A. (2011), Limits to the development of feed-forward structures in large recurrent neuronal networks, *Front. Comput. Neurosci.*, 4

Lecun, Y. (1985), Une procedure d'apprentissage pour reseau a seuil asymmetrique (a learning scheme for asymmetric threshold networks), in Proceedings of Cognitiva 85, Paris, France, 599–604

LeCun, Y., Bengio, Y., and Hinton, G. (2015), Deep learning, *Nature*, 521, 7553, 436–444

Legenstein, R. and Maass, W. (2011), Branch-specific plasticity enables self-organization of nonlinear computation in single neurons, *J. Neurosci.*, 31, 30, 10787–10802, doi:10.1523/JNEUROSCI.5684-10.2011

Litwin-Kumar, A. and Doiron, B. (2014), Formation and maintenance of neuronal assemblies through synaptic plasticity, *Nat. Commun.*, 5, 1, 1–12

Lytton, W. W., Seidenstein, A. H., Dura-Bernal, S., McDougal, R. A., Schürmann, F., and Hines, M. L. (2016), Simulation neurotechnologies for advancing brain research: parallelizing large networks in NEURON, *Neural computation*, 28, 10, 2063–2090, doi:10.1162/neco_a_00876

Maes, A., Barahona, M., and Clopath, C. (2020), Learning spatiotemporal signals using a recurrent spiking network that discretizes time, *PLoS computational biology*, 16, 1, e1007606

Markram, H., Lübke, J., Frotscher, M., and Sakmann, B. (1997), Regulation of synaptic efficacy by coincidence of postsynaptic APs and EPSPs, *Science*, 275, 213–215

Markram, H., Muller, E., Ramaswamy, S., Reimann, M. W., Abdellah, M., Sanchez, C. A., et al. (2015), Reconstruction and simulation of neocortical microcircuitry, *Cell*, 163, 2, 456–492, doi:10.1016/j.cell.2015.09.029

Mayr, C. G. and Partzsch, J. (2010), Rate and pulse based plasticity governed by local synaptic state variables, *Frontiers in Synaptic Neuroscience*, 2, 33

Morrison, A., Aertsen, A., and Diesmann, M. (2007a), Spike-timing dependent plasticity in balanced random networks, *Neural Comput.*, 19, 1437–1467, doi:10.1162/neco.2007.19.6.1437

Morrison, A., Diesmann, M., and Gerstner, W. (2008), Phenomenological models of synaptic plasticity based on spike-timing, *Biol. Cybern.*, 98, 459–478

Morrison, A., Mehring, C., Geisel, T., Aertsen, A., and Diesmann, M. (2005), Advancing the boundaries of high connectivity network simulation with distributed computing, *Neural Comput.*, 17, 8, 1776–1801, doi:10.1162/0899766054026648

Morrison, A., Straube, S., Plesser, H. E., and Diesmann, M. (2007b), Exact subthreshold integration with continuous spike times in discrete-time neural network simulations, *Neural Comput.*, 19, 1, 47–79, doi:10.1162/neco.2007.19.1.47

Nordlie, E., Gewaltig, M.-O., and Plesser, H. E. (2009), Towards reproducible descriptions of neuronal network models, *PLOS Comput. Biol.*, 5, 8, e1000456, doi:10.1371/journal.pcbi.1000456

Parker, D. (1985), Learning logic, *Technical Report TR-47*

Plesser, H., Diesmann, M., Gewaltig, M.-O., and Morrison, A. (2015), Nest: the neural simulation tool, in D. Jaeger and R. Jung, eds., Encyclopedia of Computational Neuroscience (Springer New York), 1849–1852, doi:10.1007/978-1-4614-6675-8_258

Plotnikov, D., Blundell, I., Ippen, T., Eppler, J. M., Morrison, A., and Rumpe, B. (2016), NESTML: a modeling language for spiking neurons, in Modellierung 2016 Conference, volume 254 of *LNI* (Bonner Köllen Verlag, Bonn), volume 254 of *LNI*, 93–108

Rumelhart, E., David, Hinton, E., Geoffrey, and Williams, J., Ronald (1986), Learning representations by back-propagating errors, *Nature*, 323, 533–536, doi:10.1038/323533a0

Sacramento, J., Costa, R. P., Bengio, Y., and Senn, W. (2018), Dendritic cortical microcircuits approximate the backpropagation algorithm, in Advances in Neural Information Processing Systems, 8721–8732

Sadeh, S., Clopath, C., and Rotter, S. (2015), Emergence of functional specificity in balanced networks with synaptic plasticity, *PLOS Comput. Biol.*, 11, 6, 1–27, doi:10.1371/journal.pcbi.1004307

Schmidt, M., Bakker, R., Shen, K., Bezgin, G., Diesmann, M., and van Albada, S. J. (2018), A multi-scale layer-resolved spiking network model of resting-state dynamics in macaque visual cortical areas, *PLOS Comput. Biol.*, 14, 10, e1006359, doi:10.1371/journal.pcbi.1006359

Sheik, S., Paul, S., Augustine, C., and Cauwenberghs, G. (2016), Membrane-dependent neuromorphic learning rule for unsupervised spike pattern detection, in 2016 IEEE Biomedical Circuits and Systems Conference (BioCAS) (IEEE), 164–167

Sjöström, P., Turrigiano, G., and Nelson, S. (2001), Rate, timing, and cooperativity jointly determine cortical synaptic plasticity, *Neuron*, 32, 1149–1164

Song, S., Sjöström, P., Reigl, M., Nelson, S., and Chklovskii, D. (2005), Highly nonrandom features of synaptic connectivity in local cortical circuits, *PLoS Biol.*, 3, 3, e68

Stimberg, M., Goodman, D., Benichoux, V., and Brette, R. (2014), Equation-oriented specification of neural models for simulations, *Frontiers in Neuroinformatics*, 8, 6, doi:10.3389/fninf.2014.00006

Urbanczik, R. and Senn, W. (2014), Learning by the dendritic prediction of somatic spiking, *Neuron*, 81, 3, 521–528

Werbos, P. (1974), Beyond regression : new tools for prediction and analysis in the behavioral sciences (Harvard University)

Yger, P. and Harris, K. D. (2013), The convallis rule for unsupervised learning in cortical networks, *PLOS Comput. Biol.*, 9, 10, 1–16, doi:10.1371/journal.pcbi.1003272

A: Simulation parameters		
Symbol	**Value**	**Description**
f_{pair}	$[10, 11, \ldots, 50]$ Hz	frequency of occurrence of spike pairs
Δt	± 10 ms	time shift of spike pair
w_{init} [mV]	0.5 mV or pA/ms	initial weight (unit is mV for aeif and pA/ms for hh neuron)
B: Parameters of `aeif_psc_delta_clopath`		
Symbol	**Value**	**Description**
E_L	-54.402 mV	leak reversal potential
E_{Na}	50.0 mV	sodium reversal potential
E_{K}	-77.0 mV	potassium reversal potential
g_L	30.0 nS	leak conductance
g_{Na}	$12 \cdot 10^3$ nS	sodium peak conductance
g_{K}	$3.6 \cdot 10^3$ nS	potassium peak conductance
C_m	100 pF	membrane capacitance
τ_{ex}	0.2 ms	rise time of the exc. synaptic alpha funct.
τ_{in}	2.0 ms	rise time of the inh. synaptic alpha funct.
θ_-	-64.9 mV	threshold
θ_+	-35 mV	threshold
A_{LTD}	$1 \cdot 10^{-4}$ 1/mV	amplitude of LTD
A_{LTP}	$12 \cdot 10^{-4}$ 1/mV^2	amplitude of LTP
τ_-	10 ms	time constant of $\bar{u}_-$
τ_+	114 ms	time constant of $\bar{u}_+$
τ_s	15 ms	time constant of s_j^*
d_s	5 ms	delay of $\bar{u}_\pm$
C: Parameters of `hh_psc_alpha_clopath`		
Symbol	**Value**	**Description**
E_L	-70.6 mV	leak reversal potential
g_L	30 nS	leak conductance
C_m	281 pF	membrane capacitance
V_{reset}	-60 mV	reset value of membr. pot. after spike
V_{peak}	33 mV	spike detection threshold
Δ_T	2 mV	slope factor
τ_w	144 ms	spike adaptation time constant
τ_z	40 ms	spike adaptation time constant
$V_{\text{th,max}}$	30.4 mV	threshold potential after spike
$\tau_{V,\text{th}}$	50 ms	threshold potential time constant
a	4 nS	subthreshold adaptation
b	0.0805 pA	spike triggered adaptation
θ_-	-70.6 mV	threshold of $\bar{u}_-$
θ_+	-45.3 mV	threshold of $\bar{u}_+$
A_{LTD}	$14 \cdot 10^{-5}$ 1/mV	amplitude of LTD
A_{LTP}	$8 \cdot 10^{-5}$ 1/mV^2	amplitude of LTP
τ_-	10 ms	time constant of $\bar{u}_-$
τ_+	7 ms	time constant of $\bar{u}_+$
τ_s	15 ms	time constant of s_j^*
d_s	4 ms	delay of $\bar{u}_\pm$

Table 2. Parameters of the spike pairing experiment using the Clopath rule. The values for the aeif model are taken from (**Clopath et al.**, 2010, Tab. 1 and appendix) and those for the hh model are extracted from the reference implementation by B. Torben-Nielson on ModelDB (**Hines et al.**, 2004).

A: Model summary	
Populations	Three: excitatory, inhibitory, external input
Connectivity	all-to-all, fixed out-degree, fixed in-degree
Neuron model	adaptive exponential integrate-and-fire (aeif, Clopath)
Plasticity	Clopath synapse/
Input	independent homogeneous Poisson spike trains
Measurements	synapse weight

B: Populations		
Name	**Elements**	**Population size**
E	aeif/two-comp.	$N_E = 10$
I	aeif/two-comp.	$N_I = 3$
E_{ext}	Poisson generator	$N_p = 500$

C: Connectivity			
Name	**Source**	**Target**	**Pattern**
ExcExc	E	E	all-to-all (no autapses)
ExcInh	E	I	fixed in-degree $C_E = 8$
InhExc	I	E	fixed out-degree $C_I = 6$
ExtExc	E_{Ext}	E	all-to-all
ExtInh	E_{Ext}	I	all-to-all

D: Neurons	
Name	`aeif_psc_delta_clopath`
Type	adaptive exponential integrate-and-fire
Details	see **Clopath et al.** (2010)
Parameters	see Table 4

E: Synapses			
Name	**Model**	**Initial weight [mV]**	**Max. weight [mV]**
ExcExc	`clopath_synapse`	0.25	0.75
ExcInh	`static_synapse`	1.0	–
InhExc	`static_synapse`	1.0	–
ExtExc	`clopath_synapse`	random uniform from $[0.5, 1.5]$	3.0
ExtInh	`static_synapse`	random uniform from $[0.0, 0.5]$	–

F: Input	
Type	Poisson generator
Description	homogeneous Poisson spike trains, independent for each neuron, modulated rate
Parameters	see Table 4

Table 3. Model description of Brunel network after Nordlie et al. (2009). This network is used to produce the performance measurement shown in Figure 8, Figure 9, and Figure 11. The values of the parameters are shown in Table 7.

A: Parameters of `aeif_psc_delta_clopath`		
Symbol	**Value**	**Description**
E_L	$-70.6\,\mathrm{mV}$	leak reversal potential
g_L	$30\,\mathrm{nS}$	leak conductance
C_m	$281\,\mathrm{pF}$	membrane capacitance
V_{reset}	$-60\,\mathrm{mV}$	reset value of membr. pot. after spike
V_{peak}	$20\,\mathrm{mV}$	spike detection threshold
Δ_T	$2\,\mathrm{mV}$	slope factor
τ_w	$144\,\mathrm{ms}$	spike adaptation time constant
τ_z	$40\,\mathrm{ms}$	spike adaptation time constant
$V_{\mathrm{th,max}}$	$30.4\,\mathrm{mV}$	threshold potential after spike
$\tau_{V,\mathrm{th}}$	$50\,\mathrm{ms}$	threshold potential time constant
a	$4\,\mathrm{nS}$	subthreshold adaptation
b	$0.0805\,\mathrm{pA}$	spike triggered adaptation
θ_-	$-70.6\,\mathrm{mV}$	threshold of $\bar{u}_-$
θ_+	$-45.3\,\mathrm{mV}$	threshold of $\bar{u}_+$
A_{LTD}	$14 \cdot 10^{-5}\,1/\mathrm{mV}$	amplitude of LTD
u_{ref}	60	reference value for $\bar{\bar{u}}$
$\bar{\bar{\tau}}$	$1.5 \cdot 10^3\,\mathrm{ms}$	time constant of $\bar{\bar{u}}$
A_{LTP}	$8 \cdot 10^{-5}\,1/\mathrm{mV}^2$	amplitude of LTP
τ_-	$10\,\mathrm{ms}$	time constant of $\bar{u}_-$
τ_+	$7\,\mathrm{ms}$	time constant of $\bar{u}_+$
τ_s	$15\,\mathrm{ms}$	time constant of s_j^*
d_s	$4\,\mathrm{ms}$	delay of $\bar{u}_\pm$
B: Input parameters		
Symbol	**Value**	**Description**
A_p	$60\,[\mathrm{Hz}]$	amplitude of Gaussian rate profile
σ_p	10	width of Gaussian rate profile
c_p	$0.48\,[\mathrm{Hz}]$	offset of Gaussian rate profile
s_p	$[25, 75, \ldots, 475]$	set of possible values for the center of the Gaussian μ_p
t_μ	$100\,[\mathrm{ms}]$	interval after which a new value for μ_p is drawn
N_μ	100	number of intervals t_μ

Table 4. Neuron and input parameters for simulation of network producing bidirectional connections using the Clopath rule. The values are taken from (**Clopath et al.**, 2010, Tab. 1 and appendix). The same values are used for the performance measurements shown in Figure 8 and Figure 9.

A: Simulation parameters		
Symbol	**Value**	**Description**
T_p	$1000\,\mathrm{ms}$	pattern duration
N_{rep}	100	number of pattern repetitions
N_{p}	200	number of input spike trains
f_{p}	$10\,\mathrm{Hz}$	input firing rate
w_{g_E}	$(18\,\sin(2\pi t) + 4.8)\,\mathrm{nS}$	weights to generate periodic excitatory conductance
w_{g_I}	$3\,\mathrm{nS}$	weights to generate constant inhibitory conductance
B: Parameters of `pp_cond_exp_mc_urbanczik (soma)`		
Symbol	**Value**	**Description**
C_m	$300\,\mathrm{pF}$	membrane capacitance
E_L	$-70\,\mathrm{mV}$	leak reversal potential
g_L	$30.0\,\mathrm{nS}$	leak conductance
E_{ex}	$0.0\,\mathrm{mV}$	exc. reversal potential
E_{in}	$-75.0\,\mathrm{mV}$	inh. reversal potential
τ_{ex}	$3.0\,\mathrm{ms}$	rise time of the exc. synaptic alpha funct.
τ_{in}	$3.0\,\mathrm{ms}$	rise time of the inh. synaptic alpha funct.
t_{ref}	$3.0\,\mathrm{ms}$	refractory time
C: Parameters of `pp_cond_exp_mc_urbanczik (dendrite)`		
Symbol	**Value**	**Description**
C_m	$300\,\mathrm{pF}$	membrane capacitance
E_L	$-70\,\mathrm{mV}$	leak reversal potential
g_L	$30.0\,\mathrm{nS}$	leak conductance
τ_{ex}	$3.0\,\mathrm{ms}$	rise time of the exc. synaptic alpha funct.
τ_{in}	$3.0\,\mathrm{ms}$	rise time of the inh. synaptic alpha funct.
$\phi\,(U)$	$\frac{0.15\,\mathrm{kHz}}{1+\frac{1}{2}\exp\left(\frac{-55\,\mathrm{mV}-U}{3\,\mathrm{mV}}\right)}$	rate function
g_{sp}	$600.0\,\mathrm{nS}$	coupling dendrite to soma

Table 5. Parameters of the simulation of the learning experiment using the Urbanczik-Senn rule. The same values of the neuron parameters are used for the performance measurements shown in Figure 11 and Figure 9.

A: Model summary	
Populations	Three: excitatory, inhibitory, external input
Connectivity	random with fixed indegree
Neuron model	adaptive exponential integrate-and-fire (aeif, Clopath)/ two-compartment Poisson (two-comp., Urbanczik-Senn)
Plasticity	Clopath synapse/ Urbanczik-Senn synapse
Input	independent homogeneous Poisson spike trains
Measurements	—

B: Populations		
Name	**Elements**	**Population size**
E	aeif/two-comp.	$N_E = 4N_I$
I	aeif/two-comp.	N_I
E_{ext}	Poisson generator	1

C: Connectivity				
Name	**Source**	**Target**	**Pattern**	**Weight**
Exc	E	E+I	fixed in-degree C_E	J_{ex}
Inh	I	E+I	fixed in-degree C_I	J_{in}
Ext	E_{Ext}	E+I	all-to-all	J

D: Neurons	
Name	`aeif_psc_delta_clopath`
Type	adaptive exponential integrate-and-fire
Details	see **Clopath et al.** (2010)
Parameters	see Table 4
Name	`pp_cond_exp_mc_urbanczik`
Type	two-compartment neuron with spike generation via inhomogeneous Poisson process
Details	see **Urbanczik and Senn** (2014)
Parameters	see Table 5

E: Synapses	
Name	**Model**
Exc	`clopath/urbanczik_synapse`
Inh	`clopath/urbanczik_synapse`
Ext	`static_synapse`

F: Input	
Type	**Description**
Poisson generator	homogeneous Poisson spike trains, independent for each neuron, rate $f_{ext} = \nu_{ext} C_E$

Table 6. Model description of Brunel network after Nordlie et al. (2009). This network is used to produce the performance measurement shown in Figure 8, Figure 9, and Figure 11. The values of the parameters are shown in Table 7.

A: Global simulation parameters		
Symbol	**Value**	**Description**
T	$2 \cdot 10^3$ ms	biological time
h	0.1 ms	resolution
B: Network sizes		
Symbol	**Value**	**Description**
$N = N_E + N_I$	$1.92 \cdot 10^6$	number of neurons in Clopath simulation with small indegree $K = 100$
N	$1.54 \cdot 10^5$	number of neurons in Clopath simulation with large indegree $K = 5000$
N	$3.84 \cdot 10^5$	number of neurons in Urbanczik simulation with small indegree $K = 100$
N	$3.84 \cdot 10^4$	number of neurons in Urbanczik simulation with large indegree $K = 5000$
C: Connectivity		
Symbol	**Value**	**Description**
g	7.0	ratio inh./exc. weight
J	0.1	postsynaptic amplitude The unit depends on the neuron model. In case of the aeif model and the Clopath rule it is $[\mathrm{mV}]$ and for the Urbanczik-Senn rule it is $[\mathrm{pA}]$
J_{ex}	J	amplitude of exc. postsyn. potential
J_{in}	$-gJ_{\mathrm{ex}}$	amplitude of inh. postsyn. potential
$K = C_E + C_I$	100 or 5000	total number of excitatory synapses per neuron
C_E	$0.8K$	number of excitatory synapses per neuron
C_I	$0.2K$	number of inhibitory synapses per neuron
η	0.0	learning rate
D: External input		
Symbol	**Value**	**Description**
ν_{ext}	$6.75 \cdot 10^{-3}$ Hz	factor in rate of external Poisson input $f_{\mathrm{ext}} = \nu_{\mathrm{ext}} C_E$

Table 7. Parameters of the Brunel network.